THE JOURNAL OF

VOLUME 113 · NUMBER 1 · JANUARY 1999

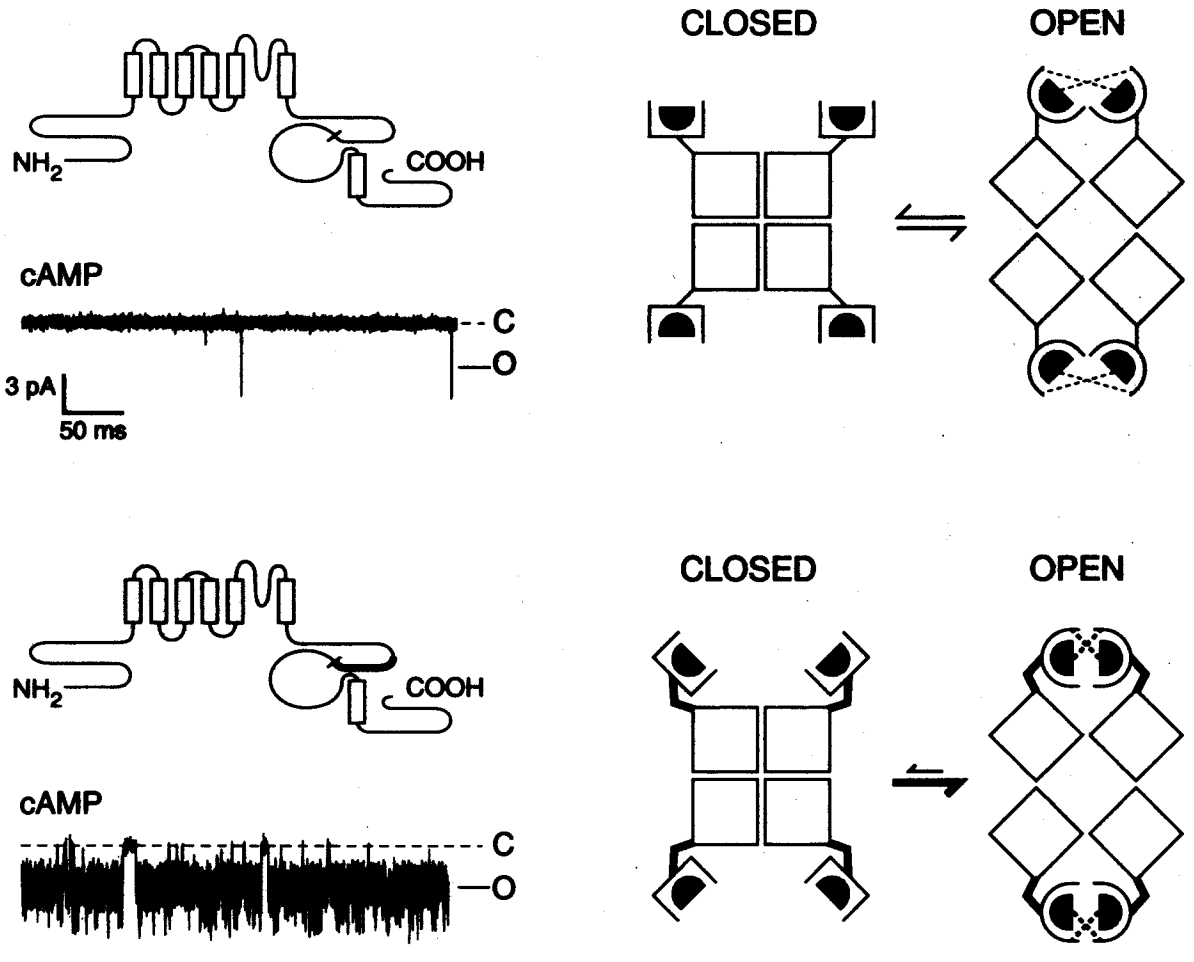

PUBLISHED MONTHLY BY The Rockefeller University Press
JGPLAD 113 (1) 1–152 (1999) ISSN 0022-1295 http://www.jgp.org

C-Linker of Cyclic Nucleotide–gated Channels Controls Coupling of Ligand Binding to Channel Gating

PIERRE PAOLETTI, EDGAR C. YOUNG, and STEVEN A. SIEGELBAUM

From the Center for Neurobiology and Behavior, Howard Hughes Medical Institute, Columbia University, New York 10032

ABSTRACT Cyclic nucleotide–gated channels are composed of a core transmembrane domain, structurally homologous to the voltage-gated K^+ channels, and a cytoplasmic ligand-binding domain. These two modules are joined by ~90 conserved amino acids, the C-linker, whose precise role in the mechanism of channel activation by cyclic nucleotides is poorly understood. We examined cyclic nucleotide–gated channels from bovine photoreceptors and *Caenorhabditis elegans* sensory neurons that show marked differences in cyclic nucleotide efficacy and sensitivity. By constructing chimeras from these two channels, we identified a region of 30 amino acids in the C-linker (the L2 region) as an important determinant of activation properties. An increase in both the efficacy of gating and apparent affinity for cGMP and cAMP can be conferred onto the photoreceptor channel by the replacement of its L2 region with that of the *C. elegans* channel. Three residues within this region largely account for this effect. Despite the profound effect of the C-linker region on ligand gating, the identity of the C-linker does not affect the spontaneous, ligand-independent open probability. Based on a cyclic allosteric model of activation, we propose that the C-linker couples the opening reaction in the transmembrane core region to the enhancement of the affinity of the open channel for agonist, which underlies ligand gating.

KEY WORDS: ligand-gated channels • cyclic GMP • cyclic AMP • activation • allosteric

INTRODUCTION

One major aim in understanding ion channel activation is to unravel the molecular mechanisms coupling a stimulus, such as voltage or ligand binding, to channel opening. In that respect, the cyclic nucleotide–gated (CNG)[1] channels, important for visual and olfactory signal transduction, are particularly interesting since they are related to both ligand- and voltage-gated channels. CNG channels are structurally homologous to the voltage-gated K^+ channels, having a series of six putative transmembrane segments interrupted between S5 and S6 by a pore-forming loop (P region) (Kaupp et al., 1989; Jan and Jan, 1990; Goulding et al., 1992). However, these channels are gated by the binding of an intracellular ligand, cAMP or cGMP, and not by voltage (Fesenko et al., 1985; Nakamura and Gold, 1987). Each CNG channel is tuned with characteristic sensitivity and selectivity for ligand, allowing optimal function in its particular physiological context. These differences among the CNG channels have proven useful in deducing the structural basis of ligand activation.

Several domains have been identified that control different aspects of ligand gating (for review, see Zagotta and Siegelbaum, 1996). Thus, a cytoplasmic cyclic nucleotide–binding (CNB) domain, formed near the COOH terminus of the channel by a stretch of ~120 residues (Kaupp et al., 1989) homologous to the cyclic nucleotide–binding domains of other proteins (Shabb and Corbin, 1992), controls the strength and selectivity of ligand binding (Altenhofen et al., 1991; Goulding et al., 1994; Varnum et al., 1995; Gordon et al., 1996; Tibbs et al., 1998). A region near the NH_2 terminus of the channel, including the S1 and S2 transmembrane segments (N-S2 domain), regulates ligand gating and the spontaneous open probability of the channel in the absence of ligand by determining the free energy difference between the unliganded open and closed states of the channel (Tibbs et al., 1997). A third region that participates in ligand gating is a highly conserved cytoplasmic stretch of ~90 residues that connects the S6 transmembrane segment to the CNB domain (the C-linker). Several individual residues or groups of residues within the C-linker have been implicated as determinants of channel activation based on studies of chemical modification (Gordon and Zagotta, 1995a,b; Broillet and Firestein, 1996; Broillet et al., 1997; Gordon et al., 1997) or amino acid substitutions (Zong et al., 1998). However, the mechanistic explanation for the role of the C-linker in channel activation remains unclear.

The cyclic allosteric model, presented in its minimal form by Monod et al. (1965), has provided a simple

Address correspondence to Steven A. Siegelbaum, Center for Neurobiology and Behavior, Howard Hughes Medical Institute, Columbia University, 722 West 168th Street, New York, NY 10032. Fax: 212-795-7997; E-mail: sas8@columbia.edu

[1] *Abbreviations used in this paper:* CNB, cyclic nucleotide–binding; CNG, cyclic nucleotide–gated; MWC, Monod-Wyman-Changeux.

framework to explain the interrelated roles of these distinct domains involved in channel gating (Goulding et al., 1994; Tibbs et al., 1997; Li et al., 1997). The cyclic model postulates that a channel can open in the absence of agonist. Agonists enhance channel opening because the channel gating reaction is coupled to a conformational change that enhances the affinity of an open channel for ligand, relative to the affinity of a closed channel. Because of thermodynamic linkage, the excess free energy of binding ("coupling energy") preferentially stabilizes the open state when agonist is bound to the channel. The efficacy of ligand activation (the opening probability of a maximally liganded channel) depends on the free energy of the intrinsic gating reaction of the channel in its unliganded form and on the amount of coupling free energy that each ligand molecule contributes to enhance opening.

The cyclic allosteric model has enabled the assignment of specific functional roles for distinct domains of the CNG channels: the CNB domain forms bonds with ligand in both the closed and open states of the channel, whereas the N-S2 domain largely determines the agonist-independent opening reaction. How does the C-linker function in this context? Is it a structural element in the intrinsic gating process, influencing the unliganded open probability? Does it directly participate in the binding reaction by forming bonds with the agonist? Does it transduce movements of gating structures into conformational changes in the CNB domain that modify agonist affinity, as suggested by the location of the C-linker in the primary amino acid sequence of the channel?

In this study, we investigated the role of the C-linker by constructing a series of chimeric channels between the bovine rod CNG channel subunit 1 (RET; Kaupp et al., 1989) and the *Caenorhabditis elegans* tax-4 CNG channel subunit (TAX-4; Komatsu et al., 1996). Despite the evolutionary distance between worms and mammals, the TAX-4 protein shares 40% overall identity with the mammalian rod and olfactory channels. Nevertheless, the TAX-4 channel is unique in its very high apparent affinity for cGMP ($K_{1/2}$ in the submicromolar range). Moreover, although the sensitivity of the TAX-4 channel to cGMP is two orders of magnitude greater than its sensitivity to cAMP, saturating doses of either ligand induce similar currents, which indicates a similar efficacy (Komatsu et al., 1996). We now report that these properties of the TAX-4 channel can be largely conferred onto the bovine rod channel by substitution of the RET C-linker sequence with the corresponding sequence from TAX-4. Much of this enhancement can be localized to the carboxy-terminal 30 amino acids of the C-linker. Within this subregion of the C-linker, substitution of three residues is sufficient to achieve a significant increase in cAMP efficacy. By measuring spontaneous channel open probability, we show that the substitution does not significantly alter the free energy of the agonist-independent opening reaction but rather increases the coupling free energy due to ligand binding. Analysis using the Monod-Wyman-Changeux (MWC) cyclic allosteric model shows a primary effect on the affinity of the open state, but not the closed state, of the channel for ligand. Thus, the C-linker is likely to couple the gating reaction to a conformational change that stabilizes cyclic nucleotide in the binding domain of an open channel.

MATERIALS AND METHODS

Molecular Biology

All channel cDNAs were subcloned into the high-expression vector pGEM-3Z containing the 5′ and 3′ *Xenopus* β globin untranslated sequences (Liman et al., 1992; Goulding et al., 1993). Point mutations were made using mismatch PCR (QuikChange; Stratagene Inc.). Chimeras were made with double PCR (Goulding et al., 1993); briefly, two PCR products generated from a RET, OLF, or TAX-4 template (see below) were isolated on gels and used as primers to generate a chimeric PCR product. Mutagenesis was followed by subcloning of minimal fragments back into the wild-type gene and complete dideoxy chain termination sequencing of the subcloned fragment. Chimeras were constructed from RET (bovine rod photoreceptor channel subunit 1; Kaupp et al., 1989), TAX-4 (*C. elegans* channel; Komatsu et al., 1996), and OLF (catfish olfactory channel subunit 1; Goulding et al., 1992). In RTC, amino acids S399–N690 of RET were replaced by S415–K733 of TAX-4. In RTB, amino acids G484–N690 of RET were replaced by G500–K733 of TAX-4. In RTL, amino acids S399–G484 of RET were replaced by S415–G500 of TAX-4. In RTL1, amino acids S399–K453 of RET were replaced by S415–K469 of TAX-4. In RTL2, amino acids Y454–G484 of RET were replaced by V470–G500 of TAX-4. In TRC, amino acids S415–K733 of TAX-4 were replaced by S399–N690 of RET. In RO133, amino acids A344–A378 of RET were replaced by S314–F448 of OLF (Goulding et al., 1993). ROPTL2 is a double chimera in which we replaced the pore of RET with that of OLF (see RO133) and the C-linker L2 of RET by that of TAX-4 (see RTL2). ROON-S2 is a double chimera in which the pore of RET is replaced by that of OLF (see RO133) and the NH_2-terminal residues N91–S240 of RET by E89–R215 of OLF (Tibbs et al., 1997).

RNAs were transcribed from NheI-linearized cDNAs using T7 RNA polymerase (Message Machine; Ambion Inc.) and injected into *Xenopus* oocytes prepared as previously described (Goulding et al., 1992). Each oocyte was injected with ~50 nl of RNA sample at 0.005–6 ng/nl (diluted concentrations yielding low expression were used for single-channel experiments).

Electrophysiology

All recordings were obtained from inside-out patches obtained from oocytes 1–10 d after injection. The pipette and bath solutions were identical and contained (mM): 67 KCl, 30 NaCl, 10 HEPES, 10 EGTA, and 1 EDTA (divalent cation-free solution; pH 7.2 with KOH). Na-cGMP or Na-cAMP (Sigma Chemical Co.) were included in the intracellular solution by iso-osmolar replacement of NaCl. Data were acquired using an Axopatch 200A amplifier (Axon Instruments), stored on VHS tape via a VR10B Digital Data Recorder (Instrutech Corp.) to an SLV420 VCR (Sony Corp.), filtered at 4 kHz (eight-pole Bessel filter, No. 902;

Frequency Devices Inc.) and digitized at 1 kHz (macroscopic currents) or 20 kHz (single-channel currents and spontaneous openings) using a TL-1 DMA interface and pCLAMP 6.0 (Axon Instruments).

Data Analysis

Macroscopic currents were analyzed with Clampfit 6.0 (Axon Instruments). Capacitive transients and leak currents obtained in solutions without cyclic nucleotide were subtracted from those obtained in the presence of cyclic nucleotides. Spontaneous increases in apparent ligand affinity (Gordon et al., 1992; Molokanova et al., 1997) and efficacy in cell-free patches were usually observed. To minimize these effects, the test response at each concentration of cyclic nucleotide was bracketed by two responses at saturating concentrations of cGMP and the test response normalized by the mean of the two maximal responses. In addition, each concentration of cyclic nucleotide was usually tested two or more times during the experiment. Current values at each concentration were then determined by averaging values obtained at different times.

Dose–response curves were measured at −80 or −100 mV. $K_{1/2}$ was estimated from fits to the Hill equation: $P_{open} = P_{max}/[1+(K_{1/2}/[A])^h]$, where $K_{1/2}$ is the apparent affinity, $[A]$ the agonist concentration, h the Hill coefficient, and P_{open} the observed open probability at a given concentration of cGMP or cAMP. P_{open} was calculated according to $P_{open} = (I/I_{max,cGMP})\ P_{max,cGMP}$, where I is the macroscopic current at a given concentration of cGMP or cAMP, $I_{max,cGMP}$ is the maximal current at a saturating concentration of cGMP, and $P_{max,cGMP}$ is the maximal open probability determined from single-channel patches in the presence of a saturating concentration of cGMP (for those constructs where we recorded single-channel currents). The lowest value of $P_{max,cGMP}$ measured was 0.91 for RET (Tibbs et al., 1997). Since TAX-4, RTC, and RTL all had $P_{max,cGMP}$ values >0.99, we assumed that all other constructs had $P_{max,cGMP} = 1$. For fits, data points were weighted by $1/P_{open}$. As the expression level of RTL was low, the mean dose–response curve of this construct was obtained from both macroscopic currents (as above) and single-channel recordings using direct measurements of P_{open}.

Single-channel recordings were analyzed by the accumulation of data points into amplitude histograms in a program written in AXOBASIC (Axon Instruments). For single-channel conductance determinations, openings during 5–10-s recording periods at +80 mV were accumulated into an amplitude histogram. For all constructs, except TAX-4, the histogram was fitted with two Gaussian functions, with one Gaussian representing the closed state and the other representing the main conducting open state. The difference between the mean of the open and closed state Gaussians was used to determine single-channel conductance. For TAX-4, due to residual proton block at +80 mV (P. Paoletti and S. Siegelbaum, unpublished data), two Gaussians were needed to fit the open states, but only the predominant, larger one was used for conductance measurements. For open probabilities, 10–20 s of continuous recordings was accumulated into an all-points amplitude histogram. The histogram was fitted with two to four Gaussian functions (depending on visual evaluation of goodness-of-fit), with one Gaussian representing the closed state and the other(s) representing up to three open states of the channel (i.e., unprotonated, singly protonated, and doubly protonated subconductance states). As these histograms include all open and closed events, the area under the closed peak represents the closed state probability (P_{closed}), and hence the open probability (P_{open}) is equal to $1 - P_{closed}$.

To obtain a quantitative description of our data, we used the MWC model as it is the simplest of the cyclic allosteric models. Although we previously found that some aspects of gating are better described by a variant of the MWC model in which the tetrameric channel gates as two independent dimers (Liu et al., 1998), the simpler MWC proves adequate to account for our macroscopic data. Qualitatively similar results are obtained using either model.

Fits to the MWC model used the equation (see Goulding et al., 1994) $P_{open} = (1 + [A]/K_o)^n/[L_0(1 + [A]/K_c)^n + (1 + [A]/K_o)^n]$, where $[A]$ is the agonist concentration, n the number of binding events, K_o and K_c are the open and closed state ligand dissociation constants, respectively, and L_0 is the allosteric equilibrium constant (see Fig. 9). In all fits, n was assumed to be 2 as this gave better fits to the data with cGMP compared with fits with four binding events (see also Fig. 4 of Tibbs et al., 1997). In the fits shown in Fig. 8, K_o is the only free parameter since L_0 is directly determined from the unliganded open probability, P_{sp}, according to $L_0 = [C]/[O] = (1/P_{sp}) - 1$. K_c is determined from the relation $K_c = K_o/[(1 - P_{max})/(P_{max}L_0)]^{1/2}$, where P_{max} is directly measured from single-channel recordings for cGMP and obtained from the following relation for cAMP: $P_{max,cAMP} = (I_{max,cAMP}/I_{max,cGMP})\ P_{max,cGMP}$.

Spontaneous channel currents were recorded for 10 s or more in the absence of ligand and accumulated in an all-points amplitude histogram. At the end of each recording of spontaneous activity, a saturating concentration of cGMP was applied to determine the number of channels present in the patch (n). n was calculated using: $n = I_{max,cGMP}/(i\ P_{max,cGMP})$, where i is the single-channel current, and where $I_{max,cGMP}$ and $P_{max,cGMP}$ were obtained as described above (all determined at −80 mV). For ROON-S2, spontaneous open probability (P_{sp}) was determined as $P_{sp} = (I_{sp}/I_{max,cGMP})P_{max,cGMP}$, where I_{sp} is the mean spontaneous current. I_{sp} was determined as the integral of the difference between the channel current and the zero current baseline (estimated by eye). For RO133 and ROPTL2, which showed very low P_{sp}, this method could not be used since large errors were introduced by estimating the zero current baseline by eye. Instead, another approach was used as described by Liu et al. (1998). In brief, the Gaussian function fit to the closed state peak was first subtracted from the raw data. Then the area of the resulting difference histogram corresponding to channel openings was divided by the entire area of the original histogram (total number of points) to yield the spontaneous open probability.

RESULTS

Activation Properties of RET and TAX-4 Differ

RET and TAX-4 display major differences in their responses to cAMP and cGMP (Fig. 1). Dose–response curves show that TAX-4 channels have a much higher sensitivity to both cAMP and cGMP than does RET (Fig. 1, top). The mean $K_{1/2}$ (concentration producing half-maximal activation) with cAMP was 28-fold lower for TAX-4 (76 μM; $n = 3$) compared with RET (2,140 μM; $n = 7$). The difference in ligand sensitivity was even more marked for cGMP, where the $K_{1/2}$ for TAX-4 (0.4 μM; $n = 6$) was 110-fold lower than that for RET (45 μM; $n = 9$). This sensitivity of TAX-4 to cGMP is the highest for any of the known CNG channels. Despite the differences in absolute $K_{1/2}$ values for ligand between RET and TAX-4, both channels display a higher sensitivity to cGMP than cAMP (RET and TAX-4

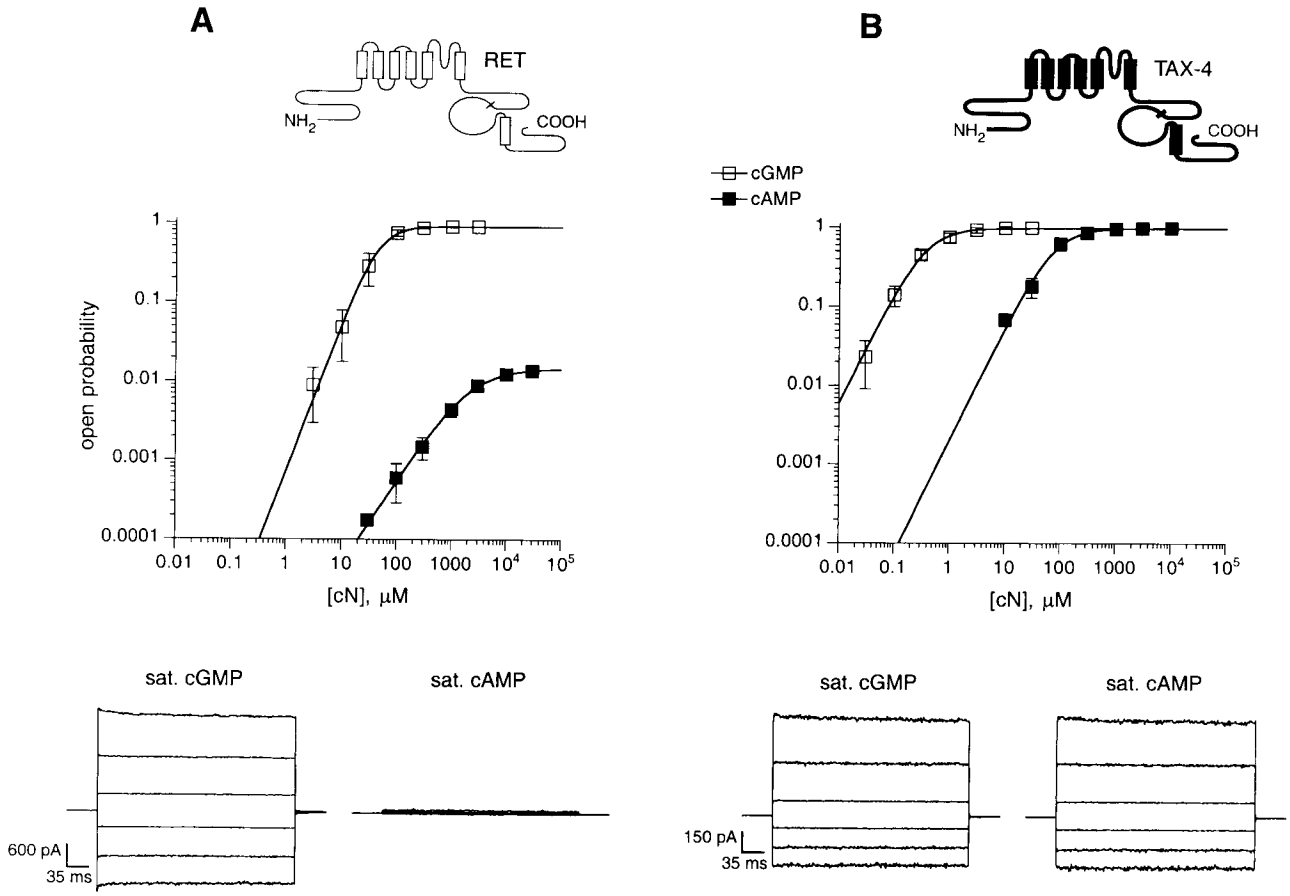

FIGURE 1. Differential activation of RET and TAX-4 by cyclic nucleotides. Activation properties of RET (A) and TAX-4 (B). Channel icons depict RET sequences as thin lines and open boxes, and TAX-4 sequences as thick lines and solid boxes. The first six rectangles represent S1–S6 membrane-spanning domains; rectangle in the COOH terminus represents the C-helix of the cyclic nucleotide–binding domain (see text) and the binding domain's NH_2 terminus is indicated by a diagonal line. (Top) Dose–response curves in response to cGMP (□) and cAMP (■). Error bars represent SEM. Data points were fitted with the Hill equation (lines), $P_{open} = P_{max}/[1 + (K_{1/2}/[A])^h]$, where $K_{1/2}$ is the apparent affinity, $[A]$ the agonist concentration and h the Hill coefficient. $K_{1/2}$ and h were as follows. For RET: 45 μM and 1.9 for cGMP, and 2,140 μM and 1.1 for cAMP. For TAX-4: 0.4 μM and 1.4 for cGMP, and 76 μM and 1.4 for cAMP. (Bottom) Representative leak-subtracted current records elicited at saturating concentrations of cGMP (300 μM for RET and 30 μM for TAX-4) or cAMP (10 mM) by voltage pulses from 0 mV to potentials between +100 and −100 mV in 40-mV steps. For RET, each trace represents an individual response to cGMP or cAMP. For TAX-4, each trace is the average of three records.

having, respectively, ~50- and ~200-fold lower $K_{1/2}$ values for cGMP than cAMP). This observation is consistent with the fact that the key residue of RET that confers cGMP selectivity (D604, located on the C-helix of the CNB domain; Varnum et al., 1995) is conserved at the homologous position in TAX-4 (D620).

Another striking difference between the activation of RET and TAX-4 is the efficacy with which cAMP activates the channel at saturating concentrations compared with the maximal activation by cGMP. Whereas cAMP acts as a partial agonist on RET channels, activating only 1.5% of the maximal current elicited by cGMP, TAX-4 channels are fully activated by cAMP (99% of response to cGMP) (Fig. 1).

TAX-4 and RET also differ in terms of their voltage dependence, with TAX-4 steady state currents showing a larger outward rectification (Fig. 1, bottom). This rectification could either be due to a strong, voltage-dependent proton block of the pore that is known to occur in CNG channels (Goulding et al., 1992; Root and MacKinnon, 1994) or to an intrinsic voltage dependence of the gating reaction. To distinguish between these two possibilities, we performed experiments using a low external H^+ concentration (pH 9.0 vs. normal pH of 7.2). Under such conditions, the TAX-4 current–voltage relationship was nearly linear (data not shown), indicating that most, if not all, of the rectification with TAX-4 arises from voltage-dependent

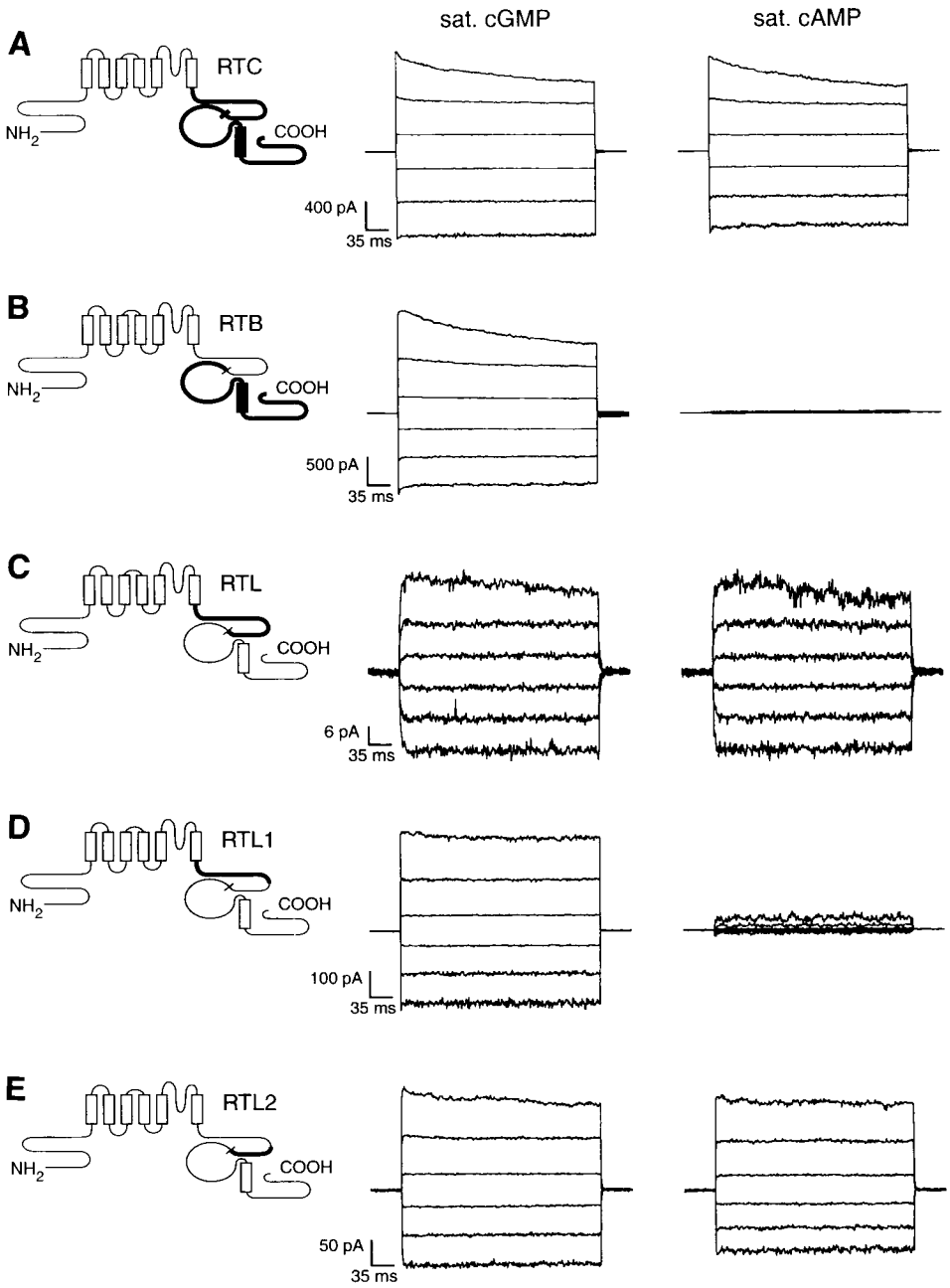

FIGURE 2. The C-linker of TAX-4 confers high cAMP efficacy. Leak-subtracted current records shown for a series of TAX-4:RET chimeras. Currents were obtained at saturating concentrations of cGMP (middle) or cAMP (right) using the same voltage protocol as in Fig. 1. 300 μM cGMP and 10 mM cAMP were used for all constructs except RTC (30 μM cGMP and 3 mM cAMP). For RTC and RTL1, each trace is an individual record; for RTB, RTL, and RTL2, each trace is the average of three records.

proton block. This effect was not studied further. Rather, we next investigated the structural determinants responsible for the remarkably high gating efficiency of the TAX-4 channels.

Identification of a Region of TAX-4, the C-Linker, Conferring High Ligand Efficacy and Sensitivity

To identify domains of the channel responsible for the differences between RET and TAX-4 in the efficacy of cAMP relative to cGMP, we constructed chimeric channels by replacing cytoplasmic COOH-terminal regions of RET with the homologous regions of TAX-4. We first replaced the entire cytoplasmic COOH-terminal region of RET, which contains the cyclic nucleotide–binding site, by that of TAX-4, yielding the chimera RTC (RET with TAX-4 C-terminus). Like TAX-4, but unlike RET, cAMP activated RTC with a high efficacy that is comparable with that of cGMP (Fig. 2 A). Surprisingly, the effect of the COOH-terminal domain is not mediated by the 120 amino acid CNB domain because a chimeric RTB (RET channel with the TAX-4 CNB domain) has a very low efficacy of activation with cAMP (Fig. 2 B).

In contrast, when the C-linker of RET is replaced by that of TAX-4 to generate the complementary chimera, RTL, cAMP functions as a full agonist with a very high

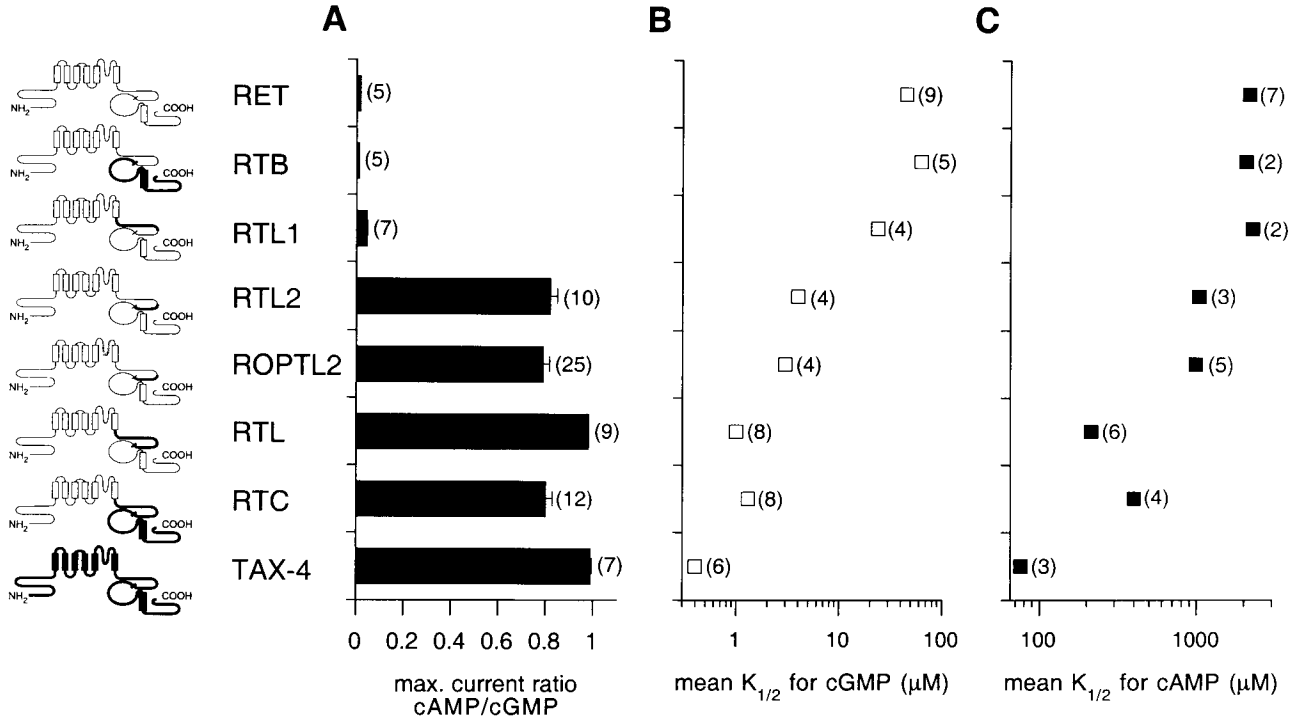

FIGURE 3. The C-linker of TAX-4 confers high apparent affinity for cAMP and cGMP. Channel notations as in Fig. 1. The thick gray line in ROPTL2 icon indicates the pore domain of OLF (see text). (A) Ratio of the maximal currents elicited by saturating concentrations of cAMP and cGMP for RET:TAX-4 chimeras. cGMP was applied at concentrations ≥30 μM for RTL2, ROPTL2, RTL, RTC, and TAX-4 and ≥300 μM for RET, RTB, and RTL1. cAMP was applied at concentrations ≥3 mM for RTL, RTC, and TAX-4 and at 10 mM for all other constructs. Currents were measured at −80 or −100 mV. The number of patches for each channel are in parentheses. Error bars show standard errors. The mean values for the ratios are as follows (±SEM): 0.015 ± 0.002 (RET), 0.0092 ± 0.001 (RTB), 0.042 ± 0.003 (RTL1), 0.816 ± 0.03 (RTL2), 0.79 ± 0.03 (ROPTL2), 0.98 ± 0.004 (RTL), 0.80 ± 0.03 (RTC), and 0.99 ± 0.007 (TAX-4). (B) $K_{1/2}$ for cGMP. Mean values are: 45 μM (n = 9) for RET, 63 μM (n = 5) for RTB, 24 μM (n = 4) for RTL1, 4 μM (n = 4) for RTL2, 3 μM for ROPTL2 (n = 4), 1.0 μM (n = 8) for RTL, 1.3 μM (n = 8) for RTC, and 0.4 μM for TAX-4 (n = 6). (C) $K_{1/2}$ for cAMP. Mean values are: 2,140 μM (n = 7) for RET, 2,050 μM (n = 2) for RTB, 2,260 μM (n = 2) for RTL1, 1,035 μM (n = 3) for RTL2, 990 μM for ROPTL2 (n = 5), 213 μM (n = 6) for RTL, 400 μM (n = 4) for RTC, and 76 μM for TAX-4 (n = 3). Note that (a) an increased cAMP/cGMP maximal current ratio is paralleled by an increased apparent affinity for both cAMP and cGMP, and (b) higher sensitivity to cGMP than cAMP is conserved in all chimeras.

relative efficacy, identical to that of TAX-4 (Fig. 2 C). To localize the effect of the TAX-4 C-linker on cAMP efficacy, we subdivided the C-linker chimera in two parts. RTL1 (RET with TAX-4 C-linker region L1) contains the first 56 amino acids of the TAX-4 C-linker, whereas RTL2 (RET with TAX-4 C-linker region L2) contains the second part of the TAX-4 C-linker (30 amino acids immediately preceding the CNB domain). cAMP activated RTL2 efficiently, whereas it activated RTL1 poorly (Fig. 2, D and E). The high relative cAMP efficacy of RTL2 resembles that of RTC, RTL, or TAX-4, whereas the low cAMP efficacy of RTL1 resembles that of RET or RTB. Thus, the COOH-terminal portion of the TAX-4 C-linker, domain L2, is sufficient to confer high cAMP efficacy.

Fig. 3 A summarizes the data obtained with the different chimeras for mean efficacy of cAMP relative to cGMP. These values clearly clustered in two groups: a RET-like group with a low relative cAMP efficacy, comprising RTB and RTL1, and a TAX-4-like group comprising RTC, RTL, and RTL2. Moreover, these values of relative efficacies for cAMP directly reflect the absolute maximal efficacy (P_{max}) with which cAMP activates the channel. This is because the P_{max} values measured at saturating concentrations of cGMP on single-channel patches were found to be close to 1 (determined for RET [P_{max} = 0.91 ± 0.08, n = 5; Tibbs et al., 1997], TAX-4 [P_{max} > 0.99, n = 3], RTL [P_{max} > 0.99, n = 9], and RTC [P_{max} > 0.99, n = 2]). Thus, the C-linker of TAX-4 is sufficient to endow channels with a cAMP efficacy identical to that of TAX-4. Moreover, most, but not all, of this effect can be localized to the L2 region, the last third of the C-linker adjacent to the cyclic nucleotide–binding domain.

In parallel with the observed increase in cAMP efficacy, the TAX-4 C-linker also enhances the sensitivity to cGMP and cAMP in the chimeric channels. Thus, the $K_{1/2}$ values for both cGMP and cAMP of the three chimeras RTC, RTL, and RTL2 were significantly decreased compared with the parent RET channel (Fig. 3,

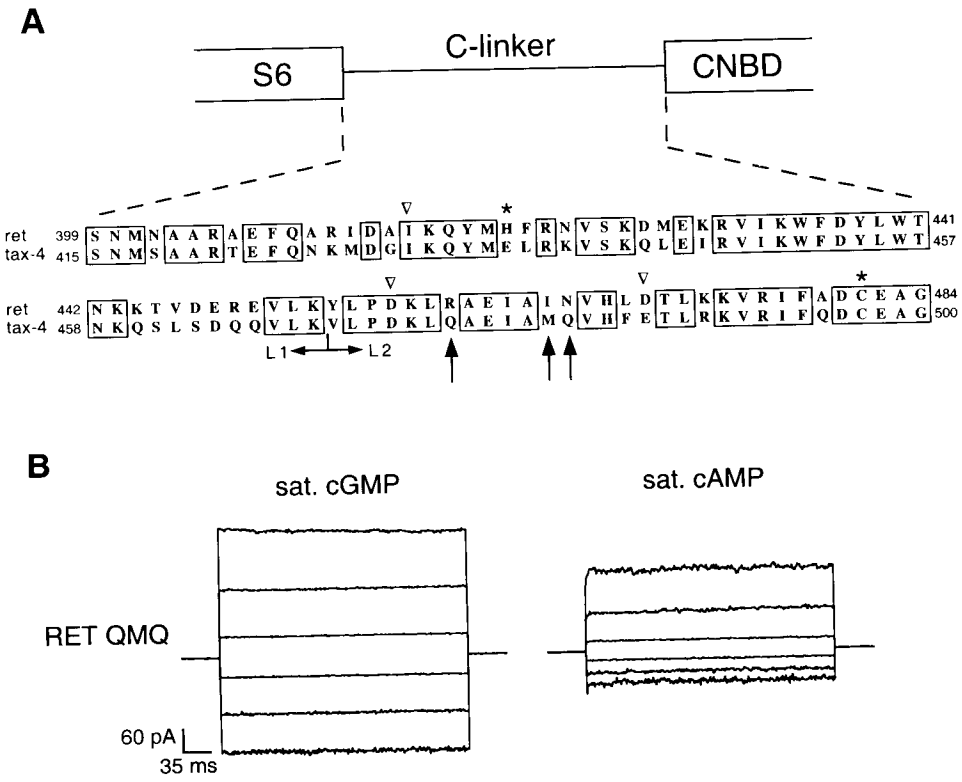

FIGURE 4. Substitution of three amino acids in the C-linker region L2 is sufficient to enhance gating properties. (A) Comparison of the amino acid sequences of the C-linker of RET and TAX-4. Identical residues are boxed and the boundary between C-linker region L1 and C-linker region L2 is shown. The percentage of identity between the two sequences is 69% for the entire region and 74% for C-linker L2 only. The two stars indicate the residues in RET previously reported to take part in channel gating (His420 [Gordon and Zagotta, 1995a]; Cys481 [Gordon et al., 1997; see also Broillet and Firestein, 1996]). ▽ mark the residues identified by Zong et al. (1998) at homologous positions in the bovine cone channel. The arrows mark the three residues identified in this study. (B) High cAMP efficacy conferred by the triple substitution RIN to QMQ in the C-linker L2 of RET (A, arrows). Currents were elicited at saturating concentrations of cGMP (1 mM) and cAMP (10 mM). Same voltage protocol as in Fig. 1. Each trace is the average of five records.

B and C). In contrast, RTB and RTL1 had mean $K_{1/2}$ values very similar to those of RET (Fig. 3, B and C).

Four major conclusions can be drawn from these results. First and most importantly, the presence of the C-linker of TAX-4 in the RTL chimera is sufficient to endow this chimera with gating properties very similar to those of the TAX-4 channel, including a high sensitivity to cGMP and high efficacy of activation with cAMP, relative to the parent RET channel. Second, the 30 amino acid COOH-terminal L2 region of the C-linker is responsible for much of the enhancement in gating properties. Third, as shown by the parallel decrease in $K_{1/2}$ values of both cAMP and cGMP, the TAX-4 C-linker enhances the sensitivity of the channel to both cyclic nucleotides. Fourth, the higher sensitivity to cGMP relative to cAMP seen with both TAX-4 and RET is conserved among all chimeras, consistent with the view that the key residue important for cGMP selectivity (D604 in RET; Varnum et al., 1995) is conserved in all constructs.

The C-linker in the chimera RTL clearly was able to confer onto RET most, but not all, of the characteristic gating properties of TAX-4. Although RTL had a mean cAMP efficacy similar to that of TAX-4 (0.98 vs. 0.99, Fig. 3), its $K_{1/2}$ values for cGMP and cAMP were two- to threefold higher than those of TAX-4 (Fig. 3). Similar discrepancies were observed for RTC. Thus, regions of TAX-4 other than the C-linker and the CNB domain must contribute to the unique gating properties of TAX-4. The influence of such regions was indeed observed in the converse chimera (TRC) in which the entire NH_2 terminus and core transmembrane domains of RET were replaced by those of TAX-4. TRC had a cAMP efficacy (mean value of 0.79 ± 0.02 [SEM], n = 4) significantly lower than that of TAX-4 (0.99), but still much higher than that of RET (0.015). TRC also displayed $K_{1/2}$ values for cAMP (mean $K_{1/2}$ of 990 μM, n = 4) and cGMP (mean $K_{1/2}$ of 4.7 μM, n = 4) intermediate between TAX-4 and RET. In this study, we have restricted our attention to the striking effects produced by substitution of the C-linker alone.

Three Amino Acid Substitution in the C-Linker L2 Region of RET Confers Enhanced Gating Properties

Which of the 86 amino acid residues of the C-linker are most critical for the enhanced gating seen with the TAX-4 region? The RET and TAX-4 C-linkers residues share an overall identity of 69% (Fig. 4 A). Interestingly, the L2 region that we identified above as crucial for conferring high cAMP efficacy and cGMP apparent affinity is even more highly conserved (74% identity).

TABLE I

Effect of Mutations in the C-Linker Region L2 of RET on cAMP Relative Efficacy

	RET	Y455V	R460Q	MQ	QMQ	L469F	D470E	K473R	A479Q	RTL2	TAX-4
I_{cAMP}/I_{cGMP}	0.015	0.021	0.036	0.045	0.31	0.022	0.022	0.009	0.009	0.82	0.99
SEM	0.002	0.0015	0.006	0.006	0.022	0.0055	0.007	0.001	0.0015	0.03	0.007
n	5	3	3	4	5	3	3	3	2	10	7

Currents were elicited at −80 mV with saturating concentrations of cGMP (30 μM for TAX-4 and ≥300 μM with all other channels) or cAMP (≥3 mM). For each construct, the mean maximal current ratio, I_{cAMP}/I_{cGMP}, and the SEM are given. The number of experiments for each construct is given in parentheses. MQ is the double mutant I465M/N466Q. QMQ is the triple mutant that also contains R460Q.

Given that only 8 of 30 residues differed between TAX-4 and RET in the L2 region, we substituted individual amino acids in the RET C-linker L2 regions with the corresponding TAX-4 residues. The effects of the different mutations on the relative cAMP efficacy are presented in Table I.

As expected from the RTL2 gating phenotype, most of the single point mutants, as well as the double mutant RET MQ (RET:I465M/N466Q), showed an increase in cAMP efficacy compared with that of RET. However, the effects were modest, ranging from a 1.4-fold increase in cAMP efficacy with the Y455V mutant to a maximal threefold increase with the double mutant RET MQ (compared with the 55-fold increase between RET and RTL2). Can these relatively small changes in cAMP efficacy caused by mutating one or two residue(s) at a time quantitatively account for the large increase in efficacy with RTL2? To approach this question, we assumed that at saturating concentrations of cAMP, channels exist in one of two states, a fully ligand-bound closed state (A_nC) and a fully ligand-bound open state (A_nO). Transitions between the two states are governed by the gating equilibrium constant, $I_{eff} = [A_nC]/[A_nO]$, which is given by $(1 - P_{max})/P_{max}$. For RET, I_{eff} with cAMP is equal to 70, whereas for RTL2 I_{eff} is equal to 0.22, a 320-fold difference. If the energetic effects of each of the individual mutants were additive (so that changes in I_{eff} would be multiplicative), we predict that the combined effects of substituting all eight residues simultaneously would only decrease the gating equilibrium constant with cAMP by a factor of 15-fold. This is far less than the experimentally observed 320-fold decrease with RTL2, indicating important synergistic interactions among the various substituted residues.

The double mutant RET MQ and the single mutant RET R460Q clearly had the largest effects (while still modest) on cAMP efficacy (Table I). Consequently, we constructed the triple mutant RET:R460Q/I465M/N466Q (RET QMQ). As shown in Fig. 4 B and in Table I, RET QMQ displays a fairly high cAMP efficacy, yielding a I_{eff} value of 2.2, much lower than the value calculated for the two mutants RET R460Q and RET MQ combined together (8), but still much higher than that of RTL2. Enhanced gating properties of the RET QMQ mutant were also revealed from its cGMP dose–response curve, which was characterized by a mean $K_{1/2}$ value of 12 μM ($n = 5$), approximately fourfold lower than that of RET (45 μM, see Fig. 3 B). Therefore, as seen with all C-linker chimeras (see Fig. 3), the enhanced cAMP efficacy was again paralleled by an enhanced cGMP apparent affinity.

High Single-Channel Open Probability of a Chimera Containing the L2 Region of the TAX-4 C-Linker

One goal of this study is to provide a detailed analysis of the effects of the C-linker region on the energetics of channel opening and ligand binding, using a cyclic allosteric model. This requires information about the absolute efficacy of cAMP and cGMP (i.e., P_{max} values), not just relative efficacies, as well as measurements of spontaneous channel open probability, for the various constructs. We therefore compared the properties of single channels whose sequences were identical except for the presence of either the TAX-4 or RET C-linker L2 regions.

To facilitate the detection of single-channel openings, we analyzed the effects of the TAX-4 C-linker in the background of a chimeric RET channel (RO133) whose single-channel conductance (57.8 ± 1.1 pS, SD, $n = 8$; see Liu et al., 1998) is significantly larger than that of either TAX-4 (32.2 ± 1.1 pS, $n = 4$) or RET (~22 pS; Goulding et al., 1993). The chimera RO133, in which the P region of RET has been replaced by that of the large-conductance catfish olfactory channel (OLF), retains the cyclic nucleotide–gating properties of RET (Goulding et al., 1993; Liu et al., 1996; Tibbs et al., 1997). Thus, by introducing both the TAX-4 C-linker L2 region and the OLF P region into RET, we obtained a double chimera, ROPTL2, with ligand-gating properties identical to those of RTL2 (efficient gating by both cAMP and cGMP; see Fig. 3) and with a large single-channel conductance (60.5 ± 4 pS, $n = 8$) similar to that of RO133 (Fig. 5). At negative potentials (−80 mV), both RO133 and ROPTL2 show pronounced open channel noise, characterized by the presence of subconductance states due to rapid block of the pore

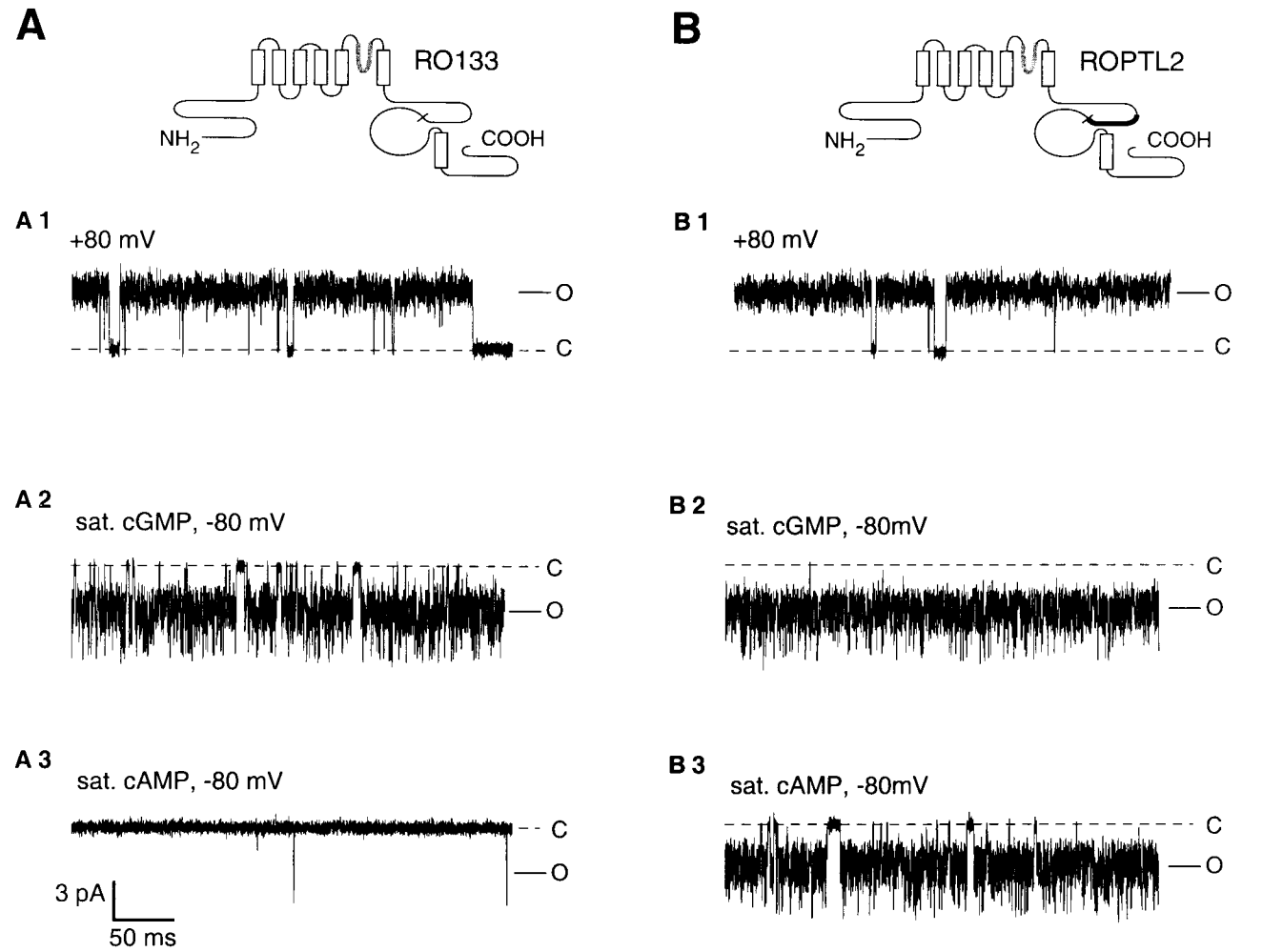

FIGURE 5. A chimera containing TAX-4 C-linker L2 region displays a high single-channel open probability in cGMP and cAMP. Representative single-channel records from inside-out patches containing a single RO133 channel (A) or a single ROPTL2 channel (B). Both chimeras contain the pore domain of OLF (see text), represented as a thick gray line. (A1 and B1) Currents at +80 mV in saturating cGMP (1 mM for RO133 [A1]) or cAMP (10 mM for ROPTL2 [B1]). (A2 and B2) Currents at −80 mV with saturating cGMP (1 mM cGMP for RO133 [A2] and 300 μM cGMP for ROPTL2 [B2]). (A3 and B3) Currents at −80 mV with saturating cAMP (10 mM). Open state (O) and closed state (C) mean currents are indicated by lines.

by external protons (Goulding et al., 1992; Root and MacKinnon, 1994). At positive potentials (+80 mV), where the above single-channel conductances were measured, the proton block–induced noise is reduced (but not eliminated) (see Fig. 5, A1 and B1).

The RO133 and ROPTL2 channels differ strikingly, however, in their activation by saturating concentrations of cAMP. RO133 exhibits very few openings with cAMP (Fig. 5 A3, $n = 3$), consistent with the low efficacy of cAMP relative to cGMP calculated from macroscopic currents (mean of 0.05 ± 0.02, SD, $n = 6$; Tibbs et al., 1997). In contrast, ROPTL2 displays a relatively high P_{max} with saturating concentrations of cAMP (0.83 ± 0.13, $n = 4$; Fig. 5 B3), consistent with the high efficacy of cAMP relative to cGMP observed with macroscopic currents (0.79 ± 0.03, $n = 25$; Fig. 3 A). This high open probability was associated with the presence of long-lived openings of the channel. With saturating concentrations of cGMP (≥1 mM), the P_{max} of RO133 was high (0.94 ± 0.03, $n = 8$; see Tibbs et al., 1997), similar to that of RET ($P_{max} = 0.91 \pm 0.08$, $n = 5$; Tibbs et al., 1997). Nonetheless, the P_{max} of ROPTL2 was even higher, with so few closures that it could not be determined reliably ($P_{max} > 0.99$, $n = 4$; compare Fig. 5, A2 and B2). P_{max} values for cGMP very close to 1 were also observed from single-channel patches for TAX-4 ($n = 3$), RTC ($n = 2$), and RTL ($n = 9$), consistent with the high efficacy associated with the TAX-4 C-linker.

Spontaneous Unliganded Open Probability Is Not Affected by the Presence of TAX-4 C-Linker L2 Region

What is the basis for the enhanced gating properties (enhanced cyclic nucleotide efficacy and apparent af-

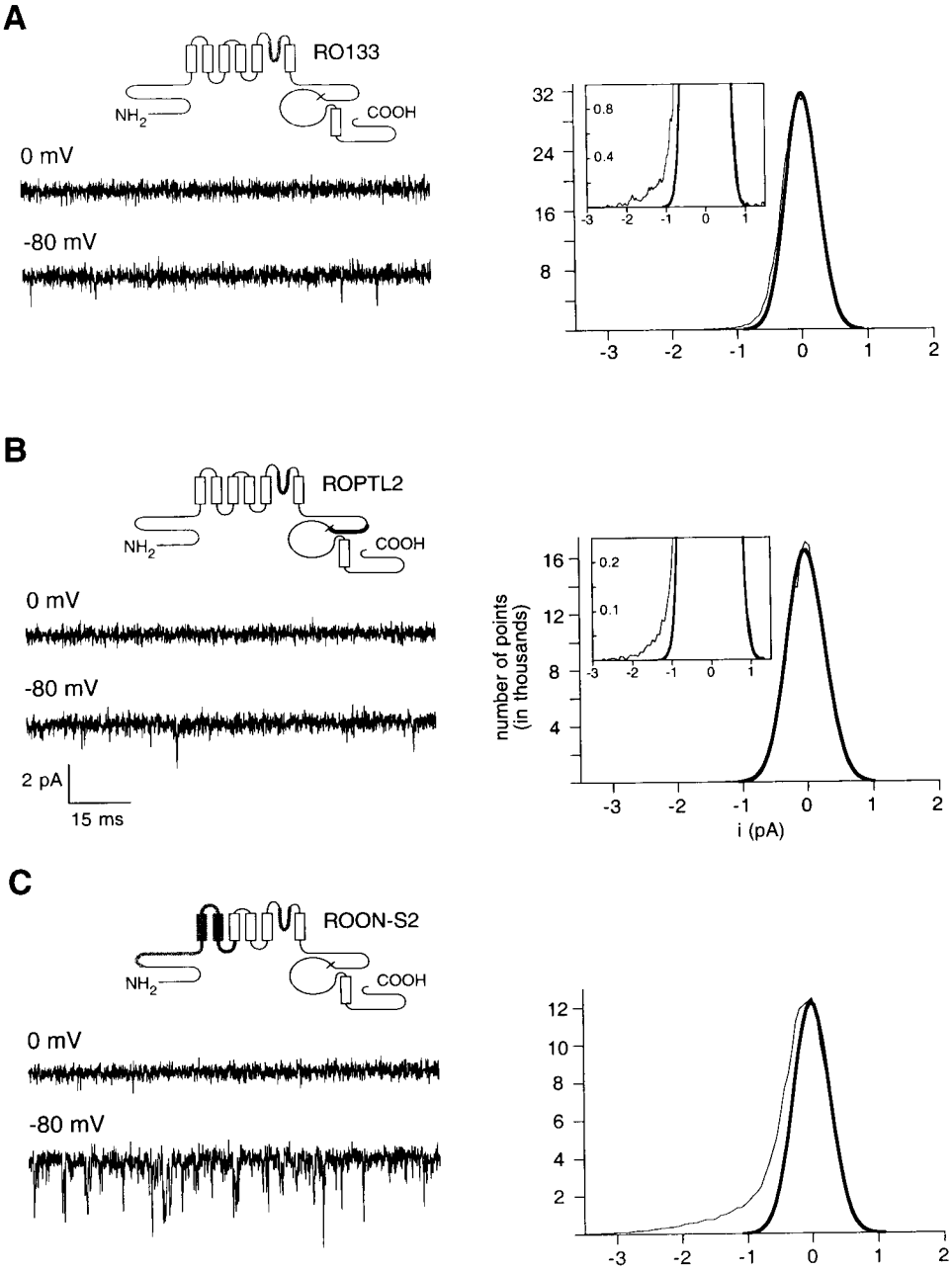

FIGURE 6. Spontaneous open probability, P_{sp}, is unaffected by the presence of the TAX-4 C-linker L2 region. Representative ligand-independent openings of RO133 (A), ROPTL2 (B), and ROON-S2 (C). ROON-S2 is a double chimera containing the pore domain and the NS-2 region of OLF (shown as thick gray lines and gray boxes; see text). (Left) Sweeps at 0 (reversal potential) and −80 mV from single patches containing 70 RO133, 60 ROPTL2, and 40 ROON-S2 channels. (Right) All-points amplitude histograms constructed from ~10 s of recordings obtained at −80 mV for each chimera. The single Gaussian function fitted to the histogram obtained at 0 mV for the same patch (representing background noise) has been scaled and superimposed as the bold line. For RO133 and ROPTL2, which have much lower spontaneous activity than ROON-S2, the increased inward current at −80 mV, compared with the noise level observed at 0 mV, is shown on an expanded scale (insets).

finity) conferred by the TAX-4 C-linker? According to the cyclic allosteric model, P_{max} can be enhanced by decreasing the energetic cost of the intrinsic opening reaction of the unliganded channel and/or by increasing the coupling free energy contributed by the binding of each ligand molecule. To distinguish between these two possibilities, we compared the intrinsic gating energetics of RO133 and ROPTL2 by measuring their ligand-independent, spontaneous open probabilities (P_{sp}). We previously showed that these probabilities directly reflect the opening reaction associated with ligand gating because changes in P_{sp} are paralleled by changes in ligand-gating properties (Tibbs et al., 1997).

Examples of spontaneous activity from individual patches are illustrated in Fig. 6. Currents were recorded in the absence of ligand at −80 and 0 mV (the reversal potential for all channels), the latter potential providing a good indicator of the patch noise. In a patch containing 70 RO133 channels, spontaneous openings at −80 mV were readily observed (compare the traces at 0 and −80 mV of Fig. 6 A), but were very infrequent. The calculated spontaneous open probability for this patch was 1.2×10^{-4}. Surprisingly, despite the enhanced ligand-dependent gating seen with ROPTL2, there was no increase in the spontaneous open probability of this channel relative to RO133.

Thus, a patch expressing 60 ROPTL2 channels also showed very infrequent spontaneous openings (probability of 0.6×10^{-4}; Fig. 6 B), very similar to the behavior of RO133. This lack of effect on P_{sp} is not due to some deficiency in our recordings since another chimera with enhanced gating that we previously studied (Tibbs et al., 1997), ROON-S2 (RET with the OLF P region and N-S2 domain), does show a large increase in P_{sp}. Thus, a patch expressing 40 ROON-S2 channels displays a P_{sp} (2.5×10^{-3}; Fig. 6 C) that is 20–40-fold higher than that of RET and ROPTL2, in agreement with previous results (Tibbs et al., 1997). For ROON-S2, this increase in P_{sp} quantitatively accounts for much of the enhancement in its ligand gating relative to RET (see Tibbs et al., 1997).

Pooled data from all spontaneous opening probability measurements obtained with RO133, ROON-S2, and ROPTL2 are shown in Fig. 7. No overlap is observed between ROON-S2 P_{sp} values and the P_{sp} values for either RO133 or ROPTL2. In contrast, P_{sp} values for RO133 and ROPTL2 completely overlapped. The mean P_{sp} value of RO133 ($1.25 \times 10^{-4} \pm 0.24 \times 10^{-4}$, $n = 23$; Tibbs et al., 1997) is not significantly different from the mean P_{sp} value of ROPTL2 ($0.89 \times 10^{-4} \pm 0.25 \times 10^{-4}$, $n = 9$). In contrast, those P_{sp} values are significantly less than the mean P_{sp} value of ROON-S2 ($2.46 \times 10^{-3} \pm 0.5 \times 10^{-3}$, $n = 13$; see Tibbs et al., 1997). Although the variability in P_{sp} measurements might obscure a small difference in the true P_{sp} of ROPTL2 compared with RO133, this difference must be much less than the 20-fold difference we detected between these channels and ROON-S2.

The two chimeras ROON-S2 and ROPTL2, both derived from the same parent channel RO133, have similar macroscopic gating properties, with a high efficacy of cAMP and high sensitivity to cGMP (for ROON-S2, see Tibbs et al., 1997). Nonetheless, the two chimeras achieve their enhanced gating relative to RO133 through strikingly different mechanisms. Thus, ROON-S2 has a lower energetic cost of channel opening due to the presence of the OLF N-S2 domain, which enhances both ligand gating and spontaneous openings (see Tibbs et al., 1997). In contrast, ROPTL2 exhibits enhanced ligand gating with no change in spontaneous openings, which implies that the L2 region of the C-linker must alter the coupling energy that ligand binding imparts to channel opening.

The C-Linker Controls the Binding of the Ligand in the Open State of the Channel

According to the cyclic allosteric model, the coupling energy provided by ligand binding arises because the open channel has a higher affinity for ligand than the closed channel. Thus, an increase in coupling energy could result from an increase in affinity of the open channel and/or a decrease in the affinity of the closed channel for ligand. To distinguish between these alternatives, we estimated the affinities of the closed and open states of the channel by analyzing dose–response curves with the minimal MWC cyclic allosteric model. According to this model, channels undergo a concerted gating reaction between a single closed (C) and open (O) state in the absence of agonist. This gating reaction is characterized by the allosteric equilibrium constant, $L_0 = [C]/[O] = (1 - P_{sp})/P_{sp}$. Agonists bind independently to either the closed or open state of the channel, with dissociation constants K_c and K_o, respectively ($K_o < K_c$). Thus, the coupling energy contributed towards channel activation upon binding of each agonist is determined by the ratio K_o/K_c. For a channel maximally occupied by n molecules of agonist, the equilibrium between the open and closed state is given by: $L_0(K_o/K_c)^n = [A_nC]/[A_nO] = (1 - P_{max})/P_{max}$, where A_nC and A_nO represent the closed and open states of the ligand-bound channel.

We first fitted dose–response relations for cAMP, since P_{max} values could be accurately measured with this ligand. In these fits, K_o is the only free parameter since L_0 is experimentally determined from P_{sp} (see Figs. 6 and 7) and K_c is constrained by the choice of K_o

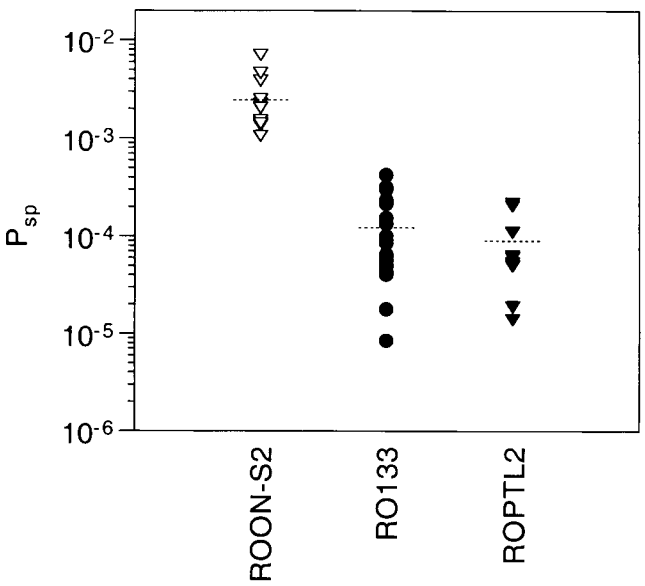

FIGURE 7. Comparison of spontaneous open probability of chimeric channels. Scatter plot of spontaneous open probability (P_{sp}) values measured at −80 mV from RO133, ROON-S2, and ROPTL2 channels. Each symbol corresponds to the value of P_{sp} obtained from an individual experiment. The mean values of P_{sp}, marked as dotted lines, are (mean ± SEM): $2.46 \times 10^{-3} \pm 0.5 \times 10^{-3}$ ($n = 13$) for ROON-S2 (see Tibbs et al., 1997), $1.25 \times 10^{-4} \pm 0.24 \times 10^{-4}$ ($n = 23$) for RO133 (Tibbs et al., 1997), and $0.89 \times 10^{-4} \pm 0.25 \times 10^{-4}$ ($n = 9$) for ROPTL2. P_{sp} for RO133 and ROPTL2 are significantly different from ROON-S2, but not from each other ($P < 0.05$, Tukey's test modified for unequal sample sizes).

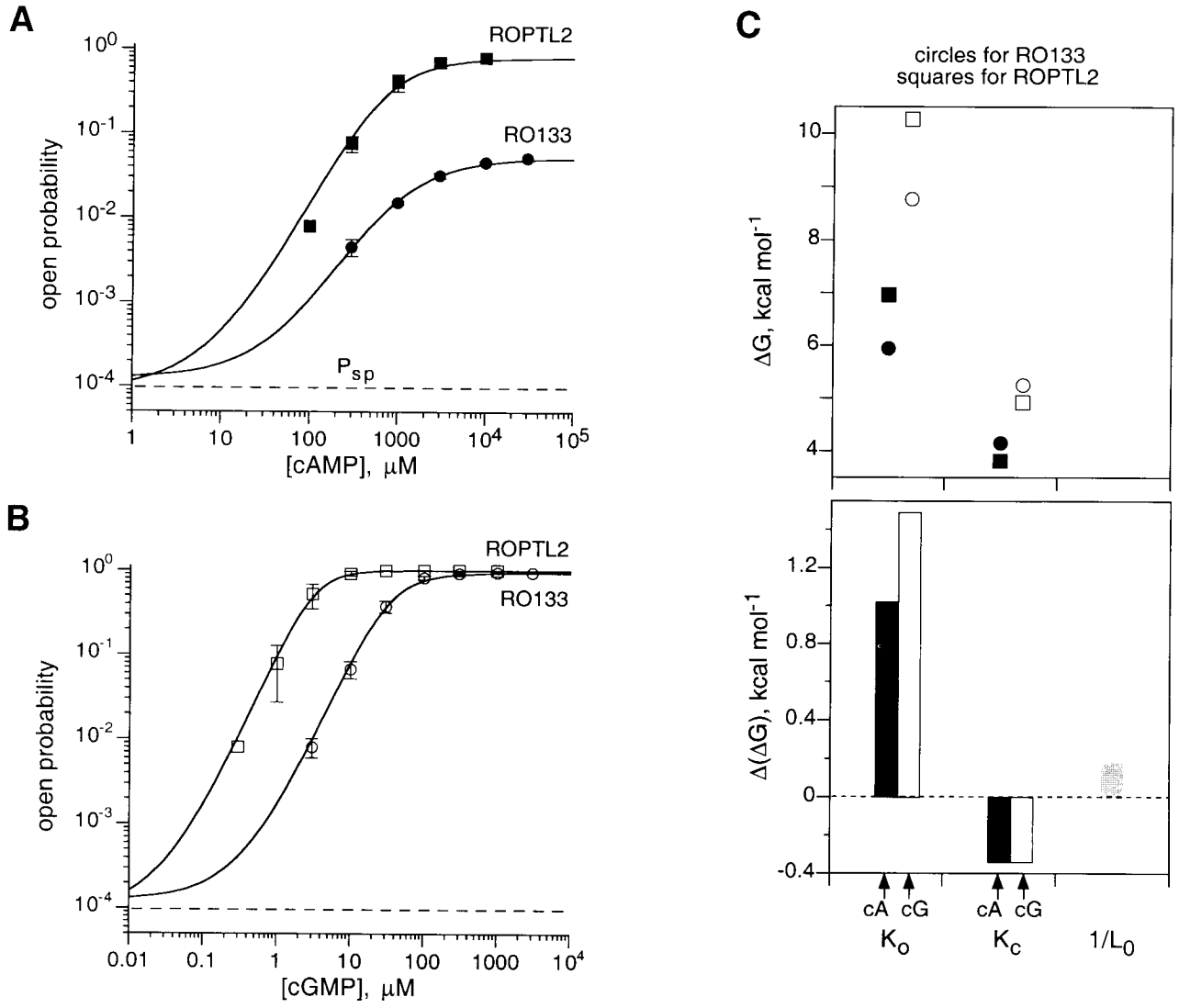

FIGURE 8. A selective decrease in K_o, the dissociation constant of the ligand from the open state, accounts for the effects of the TAX-4 C-linker L2 region. Comparison of dose–response curves for RO133 (circles) and ROPTL2 (squares) with application of cAMP (solid symbols; A) or cGMP (open symbols; B). Mean open probabilities are plotted as a function of ligand concentration. Dotted lines show the spontaneous open probability (P_{sp}) of ROPTL2. Solid lines represent fits of the MWC model to the data (see MATERIALS AND METHODS). Error bars represent standard deviation of the mean. I_0 (RO133) = 8,000, I_0 (ROPTL2) = 11,000. $P_{max,cAMP}$ = 0.051 (RO133) and 0.79 (ROPTL2). $P_{max,cGMP}$ = 0.948 (RO133). Above values for RO133 are from Tibbs et al. (1997). The fitted values of K_o were, for cAMP, 44 μM (RO133) and 7.9 μM (ROPTL2), and, for cGMP, 0.37 μM (RO133) and 0.03 μM (ROPTL2). Deduced K_c values were, for cAMP, 912 μM (RO133) and 1607 μM (ROPTL2), and, for cGMP, 141 μM (RO133) and 248 μM (ROPTL2). (C) Free energy plot (ΔG; upper part) and change in free energy plot ($\Delta(\Delta G) = \Delta G_{ROPTL2} - \Delta G_{RO133}$; lower part) of the constants K_o, K_c, and I_0. $\Delta G = -RT\ln(K)$ or $\Delta G = -RT\ln(1/I_0)$. Note that most of the changes in gating are due to a large stabilization of K_o paralleled by a smaller destabilization of K_c. In contrast, I_0 is mostly unaffected.

and the experimentally determined parameters P_{max} and P_{sp} (see MATERIALS AND METHODS). As shown in Fig. 8 A, the enhanced efficacy and sensitivity with cAMP of ROPTL2 compared with RO133 could be well accounted for by a marked decrease (approximately sixfold) in K_o paralleled by a smaller increase (~1.8-fold) in K_c. Thus, the main effect of the presence of the TAX-4 C-linker L2 domain is to stabilize the binding of cAMP to the open state of the channel. The combined effect of the changes in K_o and K_c results in an 11-fold decrease in K_o/K_c.

A qualitatively similar but even larger effect was obtained for activation with cGMP. As P_{max} values elicited by cGMP could not be accurately measured for

ROPTL2 (being too close to 1; see Fig. 5 B2), we could not constrain K_c through measurements of I_{40} and P_{max}. Rather, we assumed that the K_c values for cGMP of RO133 and ROPTL2 differed by the same factor as determined for cAMP (i.e., a 1.8-fold increase). With this assumption, the fit to the cGMP dose–response curve for ROPTL2 yielded a K_0 value more than 10-fold smaller than the one obtained for RO133 (0.03 vs. 0.37 μM; Fig. 8 B). Thus, as for cAMP, the main effect of the TAX-4 C-linker L2 domain on channel activation by cGMP is to stabilize ligand binding to the open state of the channel. These changes result in a 22-fold decrease in K_0/K_c. This conclusion is not very sensitive to our assumption of a fixed K_c value. Thus, when we explored a range of fixed K_0 values, adequate fits to the cGMP ROPTL2 dose–response curve were obtained only over a narrow range of K_0 values (0.02–0.04 μM).

Expressed as changes in free energy, the TAX-4 C-linker L2 region stabilizes the binding to the open state of the channel of cAMP and cGMP by 1.0 and 1.5 kcal/mol, respectively (Fig. 8 C). This effect is paralleled by a smaller destabilization (by ~0.4 kcal/mol) of the binding of ligand to the closed state of the channel. In contrast, the transition between the unliganded closed and open states (I_{40}) is barely affected (<0.2 kcal/mol) (Fig. 8 C). The stabilization of K_0 underlies the increased apparent affinity (i.e., decreased $K_{1/2}$) of channels containing the TAX-4 C-linker regions (see Fig. 3, B and C). The increase in coupling energy (decrease in K_0/K_c) of ~2 kcal/mol accounts for the large increases in opening equilibrium with saturating concentrations of cAMP and cGMP (see Figs. 2 and 5).

DISCUSSION

By exploiting differences in activation properties of two distantly related CNG channels, the bovine rod photoreceptor channel (RET) and a *C. elegans* sensory neuron channel (TAX-4), we have identified a region, the C-linker, that plays a major role in channel activation. The basic observation in our study is that the very high cAMP efficacy observed with TAX-4 can be conferred onto the poorly cAMP-activated RET channel by replacing the C-linker of RET by that of TAX-4. Moreover, we show that this replacement is sufficient to account for most of the enhanced gating properties (apparent affinity, absolute efficacy) observed with both cAMP and cGMP. In addition, we have localized the effect of the C-linker to a subregion of 30 amino acids (L2 region) adjacent to the CNB domain. In particular, substitution of three amino acids in this region is sufficient to significantly enhance ligand gating (Fig. 4). Secondary structure predictions show that these three amino acids are located on a putative α helix in the C-linker L2 region, spanning residues D457 to V467 in RET and D473 to V491 in TAX-4 (combined Chou-Fasman and Robson-Garnier methods).

The importance of the C-linker region in channel activation was first suggested by Gordon and Zagotta (1995a), who identified a histidine residue of RET located in the L1 region of the C-linker (H420) as the site responsible for potentiation by internal Ni^{2+}. In the rat olfactory channel, another histidine (H396), three residues apart from the "potentiating" residue, has been identified as the site responsible for an inhibitory effect of Ni^{2+} on channel gating (Gordon and Zagotta, 1995b). Later studies identified a conserved cysteine residue located at the end of the C-linker L2 sequence (C481 in RET, C460 in rat OLF) that when modified by any one of a number of sulfhydryl-reactive compounds potentiated channel activation by cyclic nucleotide (Broillet and Firestein, 1996; Gordon et al., 1997; Brown et al., 1998). However, neither the histidine nor the cysteine residues are responsible for the differences in activation observed between RET and TAX-4 since the cysteine is present in both RET and TAX-4 (Fig. 4 A) and the histidines are localized in the C-linker L1 region, whose exchange between RET and TAX-4 has little effect on channel activation (Fig. 3).

Our results are in qualitative agreement with those of Zong et al. (1998), who found, using chimeras, that the C-linker was also responsible for differences in cAMP efficacy between the rabbit olfactory channel (high efficacy) and the bovine cone photoreceptor channel (intermediate efficacy). Moreover, these authors showed that the replacement of three amino acids dispersed over the primary sequence of the cone C-linker (in both L1 and L2 regions) by the corresponding amino acids of the olfactory channel was sufficient to enhance cAMP efficacy. These residues are distinct from the C-linker residues we have identified, with two of the three residues identified by Zong et al. (1998) being conserved between RET and TAX-4 (I415 and D457 in RET, I431 and D473 in TAX-4; Fig. 4 A).

Although the varied lines of evidence discussed above all suggested that the highly conserved C-linker plays an important role in channel gating, the mechanism by which this region influences activation had not been previously identified. Here we demonstrate that the exchange of the RET and TAX-4 C-linker L2 region does not alter the spontaneous open probability of the channel, despite a large effect on ligand gating. This implies that the structural elements that participate directly in opening the channel and determine the intrinsic energetic cost of channel opening are unchanged. This renders unlikely a gate-like function for the C-linker, as has been proposed for residues immediately COOH-terminal to the S6 segment in *Shaker* K^+ channels (Liu et al., 1997). Rather, the C-linker determines the difference in agonist interactions between

open and closed states of the channel, that is, the coupling free energy. This conclusion does not depend on specification of the number of open or closed states of the channel in the cyclic allosteric model, or any assumptions of whether ligand binding is independent.

In reaching the above conclusion, we presume that spontaneous openings do indeed arise from the canonical opening reaction that operates in ligand-dependent gating. Two independent lines of evidence support this interpretation. First, exchange of the RET and OLF N-S2 region (in the chimera ROON-S2) leads to an increase in P_{sp}, which is accompanied by a parallel increase in the efficacy of cyclic nucleotides in activating the channel (Tibbs et al., 1997). Second, the NH_2-terminal inactivation peptide of the *Shaker* K^+ channel blocks the pore of CNG channels opened by ligand (Kramer et al., 1994) with an affinity similar to that with which the peptide blocks the pore of spontaneously opened channels (deduced from data of Tibbs et al., 1997). Thus, as probed by the inactivation peptide, the structure of the channel pore during spontaneous openings is similar to the structure of the channel pore during ligand-dependent openings. Therefore, P_{sp} accurately measures the energetic cost of structural changes in the transmembrane core domain during ligand-activated channel opening, and such cost is relatively insensitive to substitutions of the CNB domain (Goulding et al., 1994; Tibbs et al., 1997) or of the C-linker (this work).

Our present results, combined with previous studies, now identify three distinct domains of CNG channels with characteristic effects on channel gating. (a) The amino terminal N-S2 domain, which influences primarily the ligand-independent conformational change between closed and open states of the channel. (b) The carboxy terminal 120 amino acid CNB domain, which binds and selects ligand. (c) The C-linker, which controls the coupling between ligand binding and channel gating. (The use of chimeras does not rule out the possibility that the C-linker may also influence the ligand-independent opening reaction through residues that are conserved between TAX-4 and RET.)

Through analysis of cAMP and cGMP dose–response curves using the MWC model, we find that the C-linker preferentially influences the stability of ligand-binding to the open versus the closed state of the channel. This stabilization is similar for cAMP and cGMP, two agonists with very different affinities and efficacies for activating the channel. Thus, the stabilizing interactions in question likely involve a part of the ligand molecule common between cGMP and cAMP. The stabilization is of a magnitude ($\sim$1 kcal/mol) consistent with the participation of hydrogen bonds or van der Waals forces.

This simple model for the role of the C-linker in the gating of CNG channels can also account for the potentiating effects on ligand gating of both intracellular Ni^{2+} and sulfhydryl-reactive compounds acting on the C-linker. Indeed, such treatments increase the efficacy and apparent affinity of cAMP and cGMP (Gordon and Zagotta, 1995a, 1997; Brown et al., 1998) without altering the baseline current observed in the absence of cyclic nucleotide (our unpublished observations), a good indication of unmodified spontaneous open probabilities. In contrast, the observation that NO donors can activate olfactory channels through S-nitrosylation of the conserved cysteine in the C-linker in the absence of ligand (Broillet and Firestein, 1996; Broillet et al., 1997) does not fit in our scheme, which postulates that the presence of ligand is necessary for the C-linker to enhance gating. Direct NO activation may not be a general feature of CNG channels (see Savchenko et al., 1997) or might involve pathways different from those activated during normal ligand gating.

We considered three potential physical models for how the C-linker may stabilize ligand binding to the open state of the channel. (a) The C-linker could form direct contacts with ligand in the open state of the channel. However, in the structure of the bacterial transcription factor CAP (Weber and Steitz, 1987) and cAMP-dependent protein kinase (Su et al., 1995), cyclic nucleotide contacts only residues in the CNB domain. Moreover, our finding that individual amino acid substitutions have nonadditive effects on ligand-gating suggests that these residues do not exert their effects through direct, independent contacts with ligand. (b) The C-linker could undergo a rearrangement of its tertiary structure during gating that propagates the conformational change from the opening reaction in the transmembrane domain to a conformational change in the binding domain. Such an effect of the C-linker might be mediated by its interaction with the cytoplasmic NH_2-terminal region (Gordon et al., 1997; Varnum and Zagotta, 1997), although this interaction is not absolutely required for ligand gating (Brown et al., 1998). We disfavor this model since it implies specific interactions between disparate parts of the channel, which seem at odds with the large number of modifications of the RET C-linker that enhance gating (see above). (c) The C-linker could act passively as a rigid arm that couples a change in quaternary structure of the core region of the channel to a change in orientation of the CNB domain, which enhances ligand binding to the open state of the channel (Fig. 9).

This last possibility is consistent with a physical model of channel gating that we previously proposed, based, in part, on the x-ray crystal structure of CAP (Weber and Steitz, 1987). In CAP, which is a homodimer, a long α-helix (C-helix) forming one side of the cAMP binding pocket makes both important intrasubunit bonds with a bound cAMP, and also important inter-

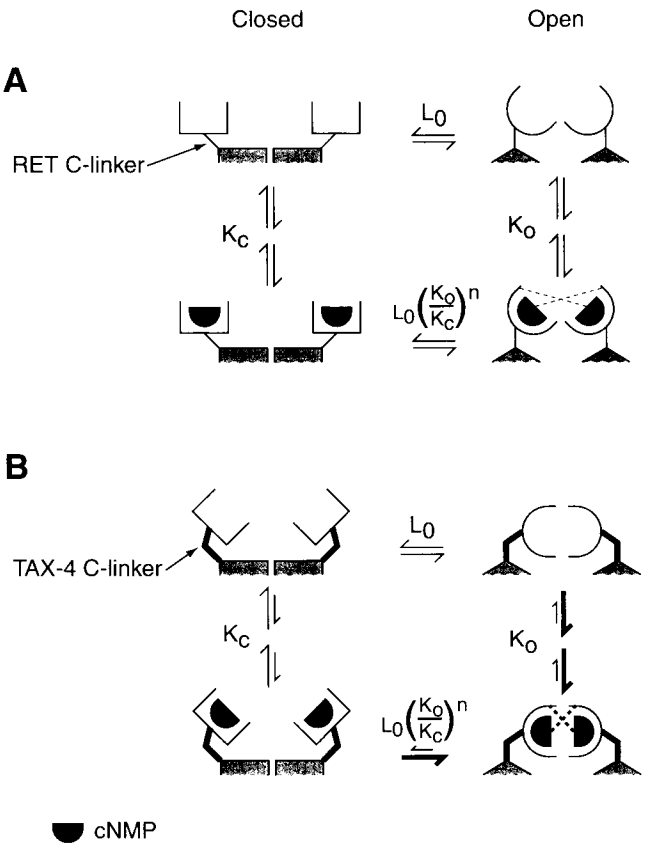

FIGURE 9. Proposed model for the influence of the C-linker region on channel activation. Each CNG channel is depicted schematically in the unliganded (top) and fully liganded (bottom) closed (left) and open (right) states. A represents RET and B represents TAX-4 or any channel containing the TAX-4 C-linker. Only two of the four subunits of a functional channel are shown. Each subunit has a core transmembrane domain (TMD, represented by a shaded rectangle, in incomplete view) and a cyclic nucleotide–binding domain (CNBD, represented by a claw). The C-linker is drawn as the connecting curve (straight line in RET channels, bent bold line in TAX-4 channels) between the TMD and the CNBD. Each CNBD binds ligand (cyclic nucleotide [cNMP], filled semicircle) independently. L_0 is the equilibrium constant for the open-to-closed transition of the unliganded channel and is determined largely by the TMD (especially the N-S2 region). In an open channel, each CNBD has a high affinity for ligand (round claw, with low dissociation constant K_o), while in a closed channel each CNBD has a lower affinity for ligand (square claw, high dissociation constant K_c). The binding of each ligand to a subunit of the channel changes the open–closed equilibrium constant relative to L_0 by a factor of K_o/K_c. In an open channel, a ligand molecule bound to one CNBD receives additional stabilization by interacting with the CNBD from an adjacent subunit (dotted lines). This additional stabilization of the open state is weaker in RET channels (higher K_o/K_c) that have a different C-linker geometry and unavailable to the unliganded channels of either species (L_0 unchanged).

subunit bonds (through S128) with cAMP bound to the neighboring subunit. Because the N-S2 domain controls the energetics of CNG channel opening (see Tibbs et al., 1997) and the corresponding region in the homologous voltage-gated K^+ channels participates in subunit assembly (Li et al., 1992; Shen et al., 1993; Babila et al., 1994), we proposed that channel opening involves a change in subunit–subunit orientation. Thus, channel opening could be readily linked to an increase in ligand affinity if the reorientation of the core region of the channel subunits were rigidly coupled (through the C-linker) to a reorientation of neighboring CNB sites, permitting C-helix–ligand intersubunit bonds to form. This model is consistent with the important role of the C-helix in CNG channel gating (Goulding et al., 1994; Varnum et al., 1995) and with recent results suggesting that the four individual subunits of a CNG channel function as a pair of dimers, with each dimer forming an independent gating unit (Liu et al., 1998).

In the context of this model, differences in C-linker structure between RET and TAX-4 would lead to different orientations between neighboring CNB sites (Fig. 9). With the TAX-4 C-linker, this orientation would permit optimal intersubunit bonds to form, whereas with the RET C-linker, the intersubunit bonds would be suboptimal. This provides an explanation for why the open-state affinity of the C-linker chimeras for ligand is greater than the open-state affinity of RET. The lower coupling energy of RET may be of physiological importance as it allows this channel to respond selectively to cGMP relative to cAMP in the concentration range appropriate to visual signal transduction.

It is an intriguing possibility that the C-linker may help determine the cyclic nucleotide sensitivity of channels other than the CNG channels, such as the related voltage-gated channels that bear a CNB motif and whose gating may be modulated by direct binding of cyclic nucleotide. These channels include the *Drosophila* ether-à-go-go channel (Brüggemann et al., 1993), the *Arabidopsis* KAT1 channel (Hoshi, 1995), or the newly cloned channels underlying the hyperpolarization-activated pacemaker currents (Santoro et al., 1997, 1998; Ludwig et al., 1998; Gauss et al., 1998). Finally, from a physiological point of view, the C-linker of CNG channels and possibly of other related proteins appears to be a domain specially suited for tuning the sensitivity of the protein to cyclic nucleotide concentrations. This could permit an optimized coupling between cellular metabolism and electrical activity.

We thank Ikue Mori for the gift of TAX-4 cDNA, Myles Akabas, David Liu, and Gareth Tibbs for helpful comments on the manuscript, Eric Odell for help in preparing Fig. 9, Arnaud Didierlaurent for help in chimera construction, and John Riley and Huan Yao for technical assistance.

Original version received 7 October 1998 and accepted version received 12 November 1998.

REFERENCES

Altenhofen, W., J. Ludwig, E. Eismann, W. Kraus, W. Bonigk, and U.B. Kaupp. 1991. Control of ligand specificity in cyclic nucleotide-gated channels from rod photoreceptors and olfactory epithelium. *Proc. Natl. Acad. Sci. USA.* 88:9868–9872.

Babila, T., A. Moscucci, H. Wang, F.E. Weaver, and G. Koren. 1994. Assembly of mammalian voltage-gated potassium channels: evidence for an important role of the first transmembrane segment. *Neuron.* 12:615–626.

Broillet, M.C., and S. Firestein. 1996. Direct activation of the olfactory cyclic nucleotide-gated channel through modification of sulfhydryl groups by NO compounds. *Neuron.* 16:377–385.

Broillet, M.-C., Y. Huang, D.H. Kamawura, and S. Firestein. 1997. Mechanisms of nitric oxide activation of olfactory cyclic nucleotide-gated channels. *Soc. Neurosci. Abs.* 23:289. (Abstr.)

Brown, R.L., S.D. Snow, and T.L. Haley. 1998. Movement of gating machinery during the activation of rod cyclic nucleotide-gated channels. *Biophys. J.* 75:825–833.

Brüggemann, A., L.A. Pardo, W. Stühmer, and O. Pongs. 1993. Ether-à-go-go encodes a voltage-gated channel permeable to K^+ and Ca^{2+} and modulated by cAMP. *Nature.* 365:445–448.

Fesenko, E.E., S.S. Kolesnikov, and A.L. Lyubarsky. 1985. Induction by cyclic GMP of cationic conductance in plasma membrane of retinal rod outer segment. *Nature.* 313:310–313.

Gauss, R., R. Seifert, and U.B. Kaupp. 1998. Molecular identification of a hyperpolarization-activated channel in sea urchin sperm. *Nature.* 393:583–587.

Gordon, S.E., D.L. Brautigan, and A.L. Zimmerman. 1992. Protein phosphatases modulate the apparent agonist affinity of the light-regulated ion channel in retinal rods. *Neuron.* 9:739–748.

Gordon, S.E., J.C. Oakley, M.D. Varnum, and W.N. Zagotta. 1996. Altered ligand specificity by protonation in the ligand binding domain of cyclic nucleotide-gated channels. *Biochemistry.* 35: 3994–4001.

Gordon, S.E., M.D. Varnum, and W.N. Zagotta. 1997. Direct interaction between amino- and carboxyl-terminal domains of cyclic nucleotide-gated channels. *Neuron.* 19:431–441.

Gordon, S.E., and W.N. Zagotta. 1995a. A histidine residue associated with the gate of the cyclic nucleotide-activated channels in rod photoreceptors. *Neuron.* 14:177–183.

Gordon, S.E., and W.N. Zagotta. 1995b. Localization of regions affecting an allosteric transition in cyclic nucleotide-activated channels. *Neuron.* 14:857–864.

Goulding, E.H., J. Ngai, R.H. Kramer, S. Colicos, R. Axel, S.A. Siegelbaum, and A. Chess. 1992. Molecular cloning and single-channel properties of the cyclic nucleotide-gated channel from catfish olfactory neurons. *Neuron.* 8:45–58.

Goulding, E.H., G.R. Tibbs, D. Liu, and S.A. Siegelbaum. 1993. Role of H5 domain in determining pore diameter and ion permeation through cyclic nucleotide-gated channels. *Nature.* 364: 61–64.

Goulding, E.H., G.R. Tibbs, and S.A. Siegelbaum. 1994. Molecular mechanism of cyclic-nucleotide-gated channel activation. *Nature.* 372:369–374.

Hoshi, T. 1995. Regulation of voltage dependence of the KAT1 channel by intracellular factors. *J. Gen. Physiol.* 105:309–328.

Jan, L.Y., and Y.N. Jan. 1990. A superfamily of ion channels. *Nature.* 345:672.

Kaupp, U.B., T. Niidome, T. Tanabe, S. Terada, W. Bonigk, W. Stühmer, N.J. Cook, K. Kangawa, H. Matsuo, T. Hirose, et al. 1989. Primary structure and functional expression from complementary DNA of the rod photoreceptor cyclic GMP-gated channel. *Nature.* 342:762–766.

Komatsu, H., I. Mori, J.S. Rhee, N. Akaike, and Y. Ohshima. 1996. Mutations in a cyclic nucleotide–gated channel lead to abnormal thermosensation and chemosensation in *C. elegans*. *Neuron.* 17: 707–718.

Kramer, R.H., E. Goulding, and S.A. Siegelbaum. 1994. Potassium channel inactivation peptide blocks cyclic nucleotide-gated channels by binding to the conserved pore domain. *Neuron.* 12:655–662.

Li, M., Y.N. Jan, and L.Y. Jan. 1992. Specification of subunit assembly by the hydrophilic amino-terminal domain of the *Shaker* potassium channel. *Science.* 257:1225–1230.

Li, J., W.N. Zagotta, and H.A. Lester. 1997. Cyclic nucleotide–gated channels: structural basis of ligand efficacy and allosteric modulation. *Q. Rev. Biophys.* 30:177–193.

Liman, E.R., J. Tytgat, and P. Hess. 1992. Subunit stoichiometry of a mammalian K^+ channel determined by construction of multimeric cDNAs. *Neuron.* 9:861–871.

Liu, D.T., G.R. Tibbs, P. Paoletti, and S.A. Siegelbaum. 1998. Constraining ligand-binding site stoichiometry suggests that a cyclic nucleotide-gated channel is composed of two functional dimers. *Neuron.* 21:235–248.

Liu, D.T., G.R. Tibbs, and S.A. Siegelbaum. 1996. Subunit stoichiometry of cyclic nucleotide–gated channels and effects of subunit order on channel function. *Neuron.* 16:983–990.

Liu, Y., M. Holmgren, M.E. Jurman, and G. Yellen. 1997. Gated access to the pore of a voltage-dependent K^+ channel. *Neuron.* 19: 175–184.

Ludwig, A., X. Zong, M. Jeglitsch, F. Hofmann, and M. Biel. 1998. A family of hyperpolarization-activated mammalian cation channels. *Nature.* 393:587–591.

Molokanova, E., B. Trivedi, A. Savchenko, and R.H. Kramer. 1997. Modulation of rod photoreceptor cyclic nucleotide–gated channels by tyrosine phosphorylation. *J. Neurosci.* 17:9068–9076.

Monod, J., J. Wyman, and J.-P. Changeux. 1965. On the nature of allosteric transitions: a plausible model. *J. Mol. Biol.* 12:88–118.

Nakamura, T., and G.H. Gold. 1987. A cyclic nucleotide–gated conductance in olfactory receptor cilia. *Nature.* 325:442–444.

Root, M.J., and R. MacKinnon. 1994. Two identical noninteracting sites in an ion channel revealed by proton transfer. *Science.* 265: 1852–1856.

Santoro, B., S.G. Grant, D. Bartsch, and E.R. Kandel. 1997. Interactive cloning with the SH3 domain of N-src identifies a new brain specific ion channel protein, with homology to eag and cyclic nucleotide–gated channels. *Proc. Natl. Acad. Sci. USA.* 94:14815–14820.

Santoro, B., D.T. Liu, H. Yao, D. Bartsch, E.R. Kandel, S.A. Siegelbaum, and G.R. Tibbs. 1998. Identification of a gene encoding a hyperpolarization-activated pacemaker channel of brain. *Cell.* 93: 717–729.

Savchenko, A., S. Barnes, and R.H. Kramer. 1997. Cyclic-nucleotide–gated channels mediate synaptic feedback by nitric oxide. *Nature.* 390:694–698.

Shabb, J.B., and J.D. Corbin. 1992. Cyclic nucleotide–binding domains in proteins having diverse functions. *J. Biol. Chem.* 267: 5723–5726.

Shen, N.V., X. Chen, M.M. Boyer, and P.J. Pfaffinger. 1993. Deletion analysis of K^+ channel assembly. *Neuron.* 11:67–76.

Su, Y., W.R. Dostmann, F.W. Herberg, K. Durick, N.H. Xuong, L. Ten Eyck, S.S. Taylor, and K.I. Varughese. 1995. Regulatory subunit of protein kinase A: structure of deletion mutant with cAMP binding domains. *Science.* 269:807–813.

Tibbs, G.R., E.H. Goulding, and S.A. Siegelbaum. 1997. Allosteric activation and tuning of ligand efficacy in cyclic-nucleotide–gated channels. *Nature.* 386:612–615.

Tibbs, G.R., D.T. Liu, B.G. Leypold, and S.A. Siegelbaum. 1998. A

state-independent interaction between ligand and a conserved arginine residue in cyclic nucleotide–gated channels reveals a functional polarity of the cyclic nucleotide binding site. *J. Biol. Chem.* 273:4497–4505.

Varnum, M.D., K.D. Black, and W.N. Zagotta. 1995. Molecular mechanism for ligand discrimination of cyclic nucleotide–gated channels. *Neuron.* 15:619–625.

Varnum, M.D., and W.N. Zagotta. 1997. Interdomain interactions underlying activation of cyclic nucleotide–gated channels. *Science.* 278:110–113.

Weber, I.T., and T.A. Steitz. 1987. Structure of a complex of catabolite gene activator protein and cyclic AMP refined at 2.5 Å resolution. *J. Mol. Biol.* 198:311–326.

Zagotta, W.N., and S.A. Siegelbaum. 1996. Structure and function of cyclic nucleotide-gated channels. *Annu. Rev. Neurosci.* 19:235–263.

Zong, X., H. Zucker, F. Hofmann, and M. Biel. 1998. Three amino acids in the C-linker are major determinants of gating in cyclic nucleotide–gated channels. *EMBO (Eur. Mol. Biol. Organ.) J.* 17: 353–362.

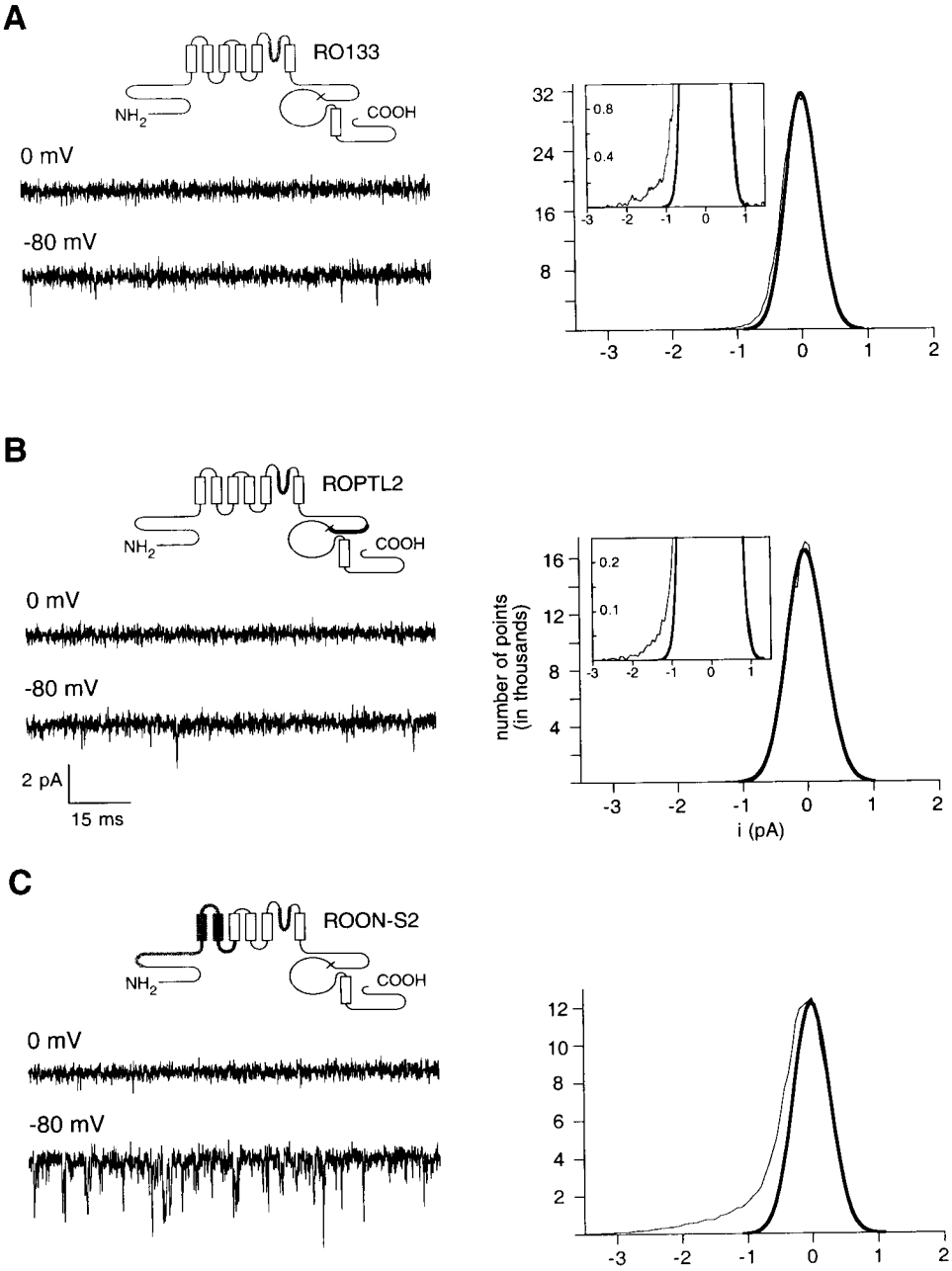

FIGURE 6. Spontaneous open probability, P_{sp}, is unaffected by the presence of the TAX-4 C-linker L2 region. Representative ligand-independent openings of RO133 (A), ROPTL2 (B), and ROON-S2 (C). ROON-S2 is a double chimera containing the pore domain and the NS-2 region of OLF (shown as thick gray lines and gray boxes; see text). (Left) Sweeps at 0 (reversal potential) and −80 mV from single patches containing 70 RO133, 60 ROPTL2, and 40 ROON-S2 channels. (Right) All-points amplitude histograms constructed from ~10 s of recordings obtained at −80 mV for each chimera. The single Gaussian function fitted to the histogram obtained at 0 mV for the same patch (representing background noise) has been scaled and superimposed as the bold line. For RO133 and ROPTL2, which have much lower spontaneous activity than ROON-S2, the increased inward current at −80 mV, compared with the noise level observed at 0 mV, is shown on an expanded scale (insets).

finity) conferred by the TAX-4 C-linker? According to the cyclic allosteric model, P_{max} can be enhanced by decreasing the energetic cost of the intrinsic opening reaction of the unliganded channel and/or by increasing the coupling free energy contributed by the binding of each ligand molecule. To distinguish between these two possibilities, we compared the intrinsic gating energetics of RO133 and ROPTL2 by measuring their ligand-independent, spontaneous open probabilities (P_{sp}). We previously showed that these probabilities directly reflect the opening reaction associated with ligand gating because changes in P_{sp} are paralleled by changes in ligand-gating properties (Tibbs et al., 1997).

Examples of spontaneous activity from individual patches are illustrated in Fig. 6. Currents were recorded in the absence of ligand at −80 and 0 mV (the reversal potential for all channels), the latter potential providing a good indicator of the patch noise. In a patch containing 70 RO133 channels, spontaneous openings at −80 mV were readily observed (compare the traces at 0 and −80 mV of Fig. 6 A), but were very infrequent. The calculated spontaneous open probability for this patch was 1.2×10^{-4}. Surprisingly, despite the enhanced ligand-dependent gating seen with ROPTL2, there was no increase in the spontaneous open probability of this channel relative to RO133.